ACS APPLIED MATERIALS & INTERFACES

Review

www.acsami.org

Nucleic Acid/Quantum Dots (QDs) Hybrid Systems for Optical and Photoelectrochemical Sensing

Ronit Freeman, Julia Girsh, and Itamar Willner*

Institute of Chemistry, Center for Nanoscience and Nanotechnologhy, The Hebrew University of Jerusalem, Jerusalem 91904, Israel

ABSTRACT: Nucleic acid/semiconductor quantum dots (QDs) hybrid systems combine the recognition and catalytic properties of nucleic acids with the unique photophysical features of QDs. These functions of nucleic acid/QDs hybrids are implemented to develop different optical sensing platforms for the detection of DNA, aptamer–substrate complexes, and metal ions. Different photophysical mechanisms including fluorescence, electron transfer quenching, fluorescence resonance energy transfer (FRET), and chemiluminescence resonance energy transfer (CRET) are used to develop the sensor systems. The size-controlled luminescence properties of QDs are further implemented for the multiplexed, parallel analysis of several DNAs, aptamer–substrate complexes, or mixtures of ions. Similarly, methods to amplify the sensing events through the biocatalytic regeneration of the analyte were developed. An additional paradigm in the implementation of nucleic acid/QDs hybrids for sensing applications involves the integration of the systems with electrodes, and the generation of photocurrents as transduction signals for the sensing events. Finally, semiconductor QDs conjugated to functional DNA machines, such as "walker" systems, provide an effective optical label for probing the dynamics and mechanical functions of the molecular devices. The present article addresses the recent advances in the application of nucleic acid/QDs hybrids for sensing applications and DNA nanotechnology, and discusses future perspectives of these hybrid materials.

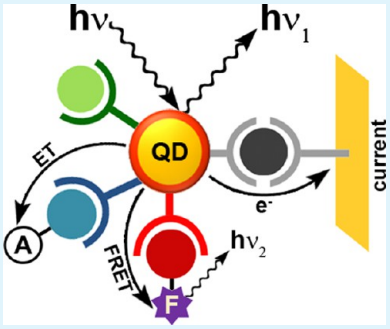

KEYWORDS: *quantum dot, DNA, nucleic acid, sensor, fluorescence, chemiluminescence, photoelectrochemistry*

1. INTRODUCTION

Semiconductor quantum dots (QDs) provide a new class of nanomaterials that reveal unique optical and electronic properties.[1] The chemistry and physics of QDs attracted substantial experimental and theoretical research efforts in the past two decades.[2−6] These studies have involved the development of synthetic methodologies for the preparation of different sized and shaped semiconductor QDs,[7−18] the surface modification of the QDs with molecular or biomolecular components,[19−44] the theoretical understanding of the optical, electronic and photophysical properties of the QDs,[1,6,45−49] and the application of the QDs in different disciplines. Different applications of semiconductor QDs were reported, including their use for energy conversion and storage,[50−53] fabrication of optoelectronic devices,[54] photocatalysis,[55−58] and particularly, sensor applications.[59−61] The rapid advances in the chemistry and physics of semiconductor QDs and their different applications were addressed in several review articles.[61−70]

The unique photophysical and chemical properties of semiconductor QDs are reflected by the following: (i) The efficient luminescence quantum yields, high brightness, and the stability of the QDs against photobleaching. (ii) The size- and shape-controlled luminescence properties of QDs originating from the quantum confinement of the electrons in the nanostructures. This allows the implementation of the same material as optical label for the parallel (multiplexed) analysis of different analytes. (iii) The luminescence spectra of the QDs reveal, usually, narrow emission bands and large Stokes shifts. This allows the effective coupling of the emitted light to other fluorophores or QDs. (iv) In contrast to organic fluorophores or transition metal complexes that exhibit broad absorbance bands and require specific wavelength excitation, QDs can be excited by a common high-energy excitation wavelength, leading to the size-controlled luminescence. This allows the multiplexed detection of analytes through excitation of different sized QDs at a single wavelength, while designing sensing platforms with low background interferences. (v) The capping layer stabilizing the QDs can be used as a functional interface for the tethering of chemical recognition sites. This is particularly important for QDs stabilized in aqueous media that allows the attachment of biological recognition sites (nucleic acids, antibodies, enzymes) and the development of bioanalytical sensing platforms in aqueous environments.

The optical functions of semiconductor QDs originate from the photoexcitation of the QDs and the transfer of valence-band electrons to the conduction-band. The resulting electron–hole species may then be utilized by different mechanisms for sensing applications, as schematically outlined in Figure 1. The radiative recombination of the electron–hole

Special Issue: Forum on Biomedical Applications of Colloidal Photoluminescent Quantum Dots

Received: December 23, 2012
Accepted: February 20, 2013
Published: February 20, 2013

 © 2013 American Chemical Society

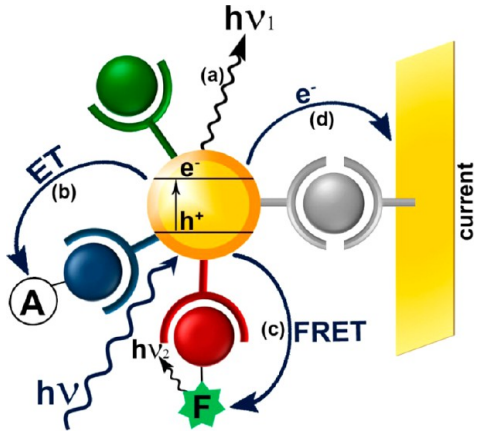

Figure 1. Schematic representation of different QD-based sensing configurations using (a) luminescence, (b) electron transfer, ET, (c) FRET, or (d) photocurrent generation as readout signals.

pair leads to the luminescence of the QDs, Figure 1, path (a). Nonetheless, in the presence of electron acceptors or electron donors the electron transfer (ET) of conduction band electrons to the acceptor units (or the donation of electrons by the donors to the valence band holes) might proceed, Figure 1, path (b). This separates the electron–hole pairs and leads to the quenching of the luminescence of the QDs via electron transfer involving secondary chemical components. Alternatively, the emitted luminescence from the QDs may provide an energy source for the fluorescence resonance energy transfer (FRET) and the excitation of a secondary chromophore, Figure 1, path (c). Finally, the integration of the QDs with an electrode surface might lead to the injection of the photoexcited conduction-band electrons to the electrode and to the generation of photocurrents as a result of a recognition event, Figure 1, path (d).

For the operation of the electron transfer quenching mechanism the redox potential energy levels of the electron acceptor (or the redox levels of the electron donor) must be appropriately aligned in respect to the redox potential of the conduction-band (or valence-band), to allow downhill electron transfer processes. The rate-constant for electron transfer from the QDs to an electron acceptor (or the rate constant for transferring the electron from a donor to the valence-band holes) is given by eq 1, where R_o and R correspond to the van der Waals distance and actual distance separating the electron acceptor (or electron donor) and the QDs, β is the electronic coupling constant, ΔG° is the free energy change associated with the electron transfer, and λ is the reorganization energy accompanying the electron transfer process.

$$k_{et} = \frac{4\pi^2}{h}(T^0_{DA})^2 e^{-\beta(R-R_0)} \frac{1}{\sqrt{4\pi\lambda K_B T}} e^{-(\Delta G^0+\lambda)^2/4\pi K_B T} \quad (1)$$

The fluorescence resonance energy transfer (FRET) is a further photophysical mechanism to follow recognition events, and particularly useful to probe the dynamics of the formation of recognition complexes. The FRET process involves dipole–dipole interactions between a donor–acceptor pair.[71] The process is sensitive to the distance separating the donor–acceptor pair, and thus provides a versatile spectroscopic tool to follow recognition events at intimate contact. The FRET efficiency, E, between a donor–acceptor pair separated by the distance r is given by eq 2, where R_o is the Förster radius that is calculated by eq 3, where K^2 is a relative orientation parameter of the two dipoles (K^2 is 2/3 for two randomly oriented dipoles), QY_D corresponds to the luminescence quantum yield of the donor fluorohpore, n is the refractive index of the system, and $J(\lambda)$ represents the spectral overlap integral between the emission spectrum of the donor and the absorbance spectrum of the acceptor. The overlap integral is calculated using eq 4, where $\varepsilon_A(\lambda)$ is the extinction coefficient of the acceptor, and $F_D(\lambda)$ corresponds to the normalized emission spectrum. Typical Förster distances separating the donor and the acceptor range between 2 and 8 nm. FRET signals are detectable up to about twice the Förster distance separating the donor–acceptor pair. If, however, the acceptor unit is tethered to n × donor sites, the FRET efficiency increases and is given by eq 5. The different photophysical quenching mechanisms of the QDs by the electron acceptors (electron transfer (ET) or FRET) are distance-dependent, yet they show different distance-dependent functions. Although the electron transfer quenching process is effective at short distances separating the QDs and acceptor pairs, the FRET quenching mechanism may proceed at larger distances, provided that the donor exhibits a high luminescence quantum yield, and provided that an efficient spectral overlap between the donor emission and acceptor absorbance exists. This implies that the capping layer associated with the QDs should comply with the photophysical mechanism selected for the development of the specific sensor.

$$E = \frac{R_0^6}{R_0^6 + r^6} \quad (2)$$

$$R_0 = \sqrt[6]{\frac{8.8 \times 10^{-25} K^2 QY_D J(\lambda)}{n^4}} \quad (3)$$

$$J(\lambda) = \int_0^\infty \varepsilon_A(\lambda) F_D(\lambda) \lambda^4 d\lambda \quad (4)$$

$$E = \frac{nR_0^6}{nR_0^6 + r^6} \quad (5)$$

The present article addresses recent advances in the application of semiconductor QDs in DNA nanotechnology, and particularly, the application of nucleic acid/QDs hybrid systems for sensing, and specifically, for bioanalytical applications in medicine. The base sequences in nucleic acids encode functional information in the biopolymers. Besides instructive base-pairing leading to duplex DNA structures, catalytic and recognition properties can be encoded into the nucleic acid sequences. Sequence-specific nucleic acids exhibiting specific binding sites for low-molecular-weight substrates,[72−74] macromolecules, e.g., proteins, or whole cells (aptamers) can be elicited by the Systematic Evolution of Ligands by Exponential Enrichment (SELEX) process.[72−74] Similarly, numerous catalytic nucleic acids (DNAzymes) duplicating native enzymes or catalyzing new chemical transformations were developed.[75−77] Also, natural or synthetic pyrimidine and purine bases bind metal ions,[78−81] e.g., formation of thymine-Hg^{2+}-thymine complexes,[78,79] and such complexes can participate cooperatively in the formation, and stabilization, of duplex nucleic acid structures. In addition, molecular entities, such as redox-active compounds can intercalate into duplex DNA structures,[82−85] and single-stranded nucleic acids might form functional nanostructures capable of binding redox-active compounds, e.g., hemin/G-quadruplexes.[86,87] These unique

features of nucleic acids provide a rich "toolbox" for the construction of sensor devices. The construction of nucleic acid-modified QDs as functional hybrid systems for sensing is dictated, however, by the nature of the target analyte and desirable sensitivity. Although the analysis of genes requires low detection limits, in the range of pM and lower, higher detection limits for certain biomarkers may be acceptable. These considerations, and particularly, development of application paths, should be taken into account upon developing the different QD-based sensors.

2. QD/NUCLEIC ACID CONJUGATES FOR THE DEVELOPMENT OF LUMINESCENT SENSORS

The unique luminescence properties of semiconductor QDs, and particularly, the size-controlled luminescence features of the QDs were used to develop DNA sensors by implementing the QDs as luminescent labels, and specifically, to design multiplexed DNA analysis platforms using different sized QDs as labels. For example, the sandwich assay using an array of nucleic acid probes for different targets was applied for the multiplexed analysis of different DNAs, Figure 2. Three

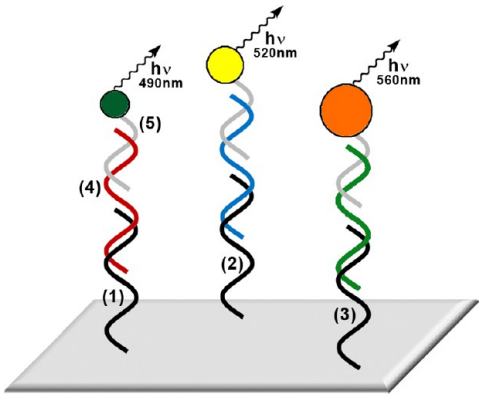

Figure 2. Application of different-sized QDs as signaling labels for multiplexed DNA hybridization and analysis on microarrays.

different probes, (**1**), (**2**), and (**3**), were used to analyze three different targets. The principle is depicted for analyzing the target (**4**) by probe (**1**). The hybridization of the target with the probe is followed by the "sandwich-type" hybridization of the nucleic acid (**5**)-modified 490 nm emitting QDs to the free single-stranded tether of the analyte. The other targets are, similarly, imaged by the respective probes by implementing different sized QDs emitting at 520 and 560 nm. Examples include the parallel analysis of hepatitis B and C with different sized CdSe/ZnS QDs.[88] Similarly, the p53 gene was detected within minutes in the presence of a background mixture consisting of single-nucleotide polymorphic sequences, using the specific nucleic acid-modified QDs that hybridize with the p53 oncogene.[88] Other related configurations[89] have been implemented for the multiplexed analysis of RNA target.

These different assays utilize the luminescence features of the QDs as reporting signals. Nonetheless, by the implementation of additional photophysical mechanisms, involving QDs, such as the electron transfer quenching of QDs, the fluorescence resonance energy transfer process in the presence of QDs, or the chemiluminescence resonance energy transfer process to QDs, sensing platforms of enhanced complexity might be envisaged. Particularly, the dynamics of hybridization and enzyme/DNAzyme-driven recognition processes involving nucleic acids might be followed by such photophysical mechanisms. Furthermore, the QDs might act as an optical carrier for numerous probe units, and thus, the development of enzyme-driven regeneration processes of the target on the QDs might lead to the sequential autonomous utilization of the numerous probe units associated with the QDs. Such biocatalytic mechanisms could provide amplification paths for the detection of DNA as aptamer/substrate complexes. These issues are discussed in the subsequent subsections.

2.1. Sensing and Multiplexed Analysis of DNA and Aptamer–Substrate Complexes by Electron Transfer, FRET, and CRET Quenching Mechanisms. Several studies have implemented the electron transfer quenching mechanism of QDs for the development of QD-based sensing platforms. The anticancer drug mitoxantrone, MTX, (**6**), adsorbs to CdTe QDs, leading to their quenching by an electron transfer mechanism.[90] In the presence of a duplex DNA, desorption of the drug from the QDs proceeds through the intercalation of the drug in the duplex DNA, Figure 3A. This leads to the

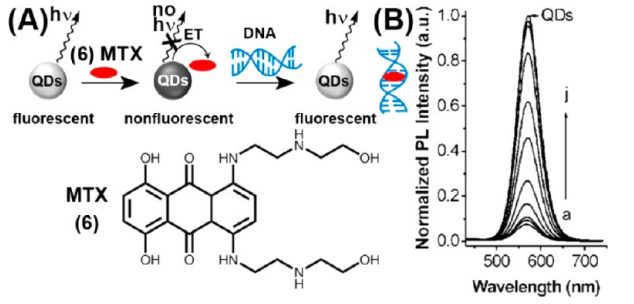

Figure 3. (A) Following the interaction of an anticancer drug and a duplex DNA using QDs as luminescent probes and electron transfer as sensing mechanism. (B) Luminescence spectra corresponding to the restoration of the luminescence of the QDs in the presence of (**6**) by the addition of different concentrations of calf thymus DNA that bind (**6**) and removes it from the surface of the QDs: (a) 0, (b) 0.81, (c) 2, (d) 4.1, (e) 8.2, (f) 12.2, (g) 16.2, (h) 24.6, (i) 32.5, and (j) 40.6 μM. Adapted with permission from ref 90. Copyright 2009 American Chemical Society.

activation of the luminescence of the QDs, Figure 3B. Although the method does not reveal high sensitivity (100 nM to 4.5 μM), the system may be useful for screening anticancer drugs, and for probing drug–DNA interactions. The intercalation of the anticancer drug doxorubicin, (**7**), into duplex nucleic acid structures, and the electron transfer quenching of CdSe/ZnS QDs by the intercalated doxorubicin, provided a general mechanism for the development of DNA sensors and aptasensors.[91] The binding of a target DNA, (**8**), to the complementary probe nucleic acid, (**9**)-functionalized CdSe/ZnS QDs, followed by the intercalation of doxorubicin to the resulting hybrids, resulted in the quenching of the luminescence of the QDs, Figure 4A, B. The method enabled the detection of the target DNA with a sensitivity corresponding to 10 nM. This electron transfer quenching mechanism was further implemented to develop QD-based aptasensors.[91] For example, the anti-thrombin aptamer nucleic acid sequence, (**10**), was linked to CdSe/ZnS QDs, Figure 4C, and the aptamer sequence was blocked by a complementary nucleic acid, (**11**). The intercalation of doxorubicin into the blocked duplex structure (**10**)/(**11**) led to the electron transfer quenching of the QDs. In the presence of thrombin, the blocker units were separated from the aptamer chains, due to the formation of the aptamer–

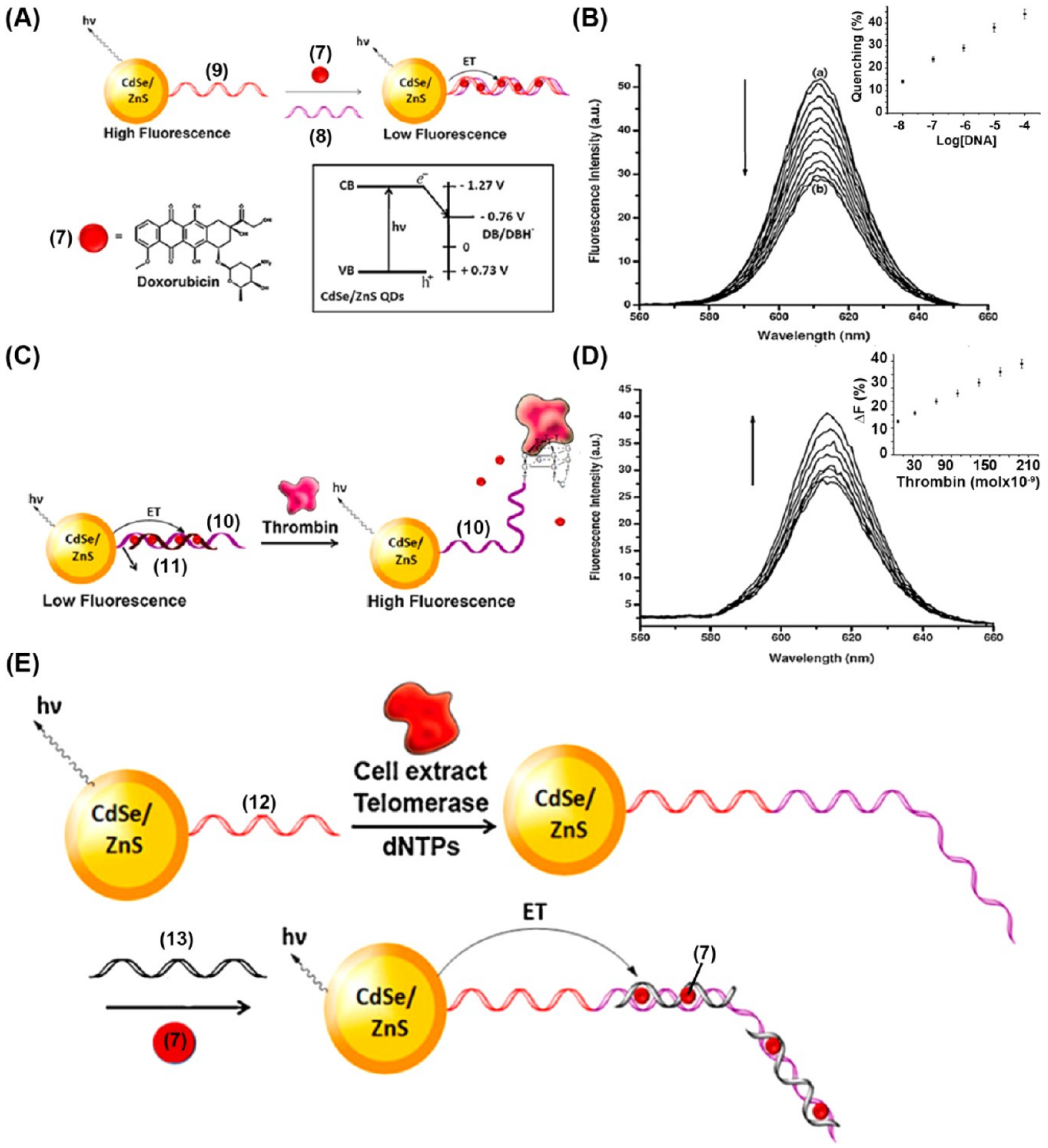

Figure 4. (A) Sensing the target DNA (**8**) by the probe nucleic acid (**9**)-modified QDs, using doxorubicin (**7**) as an electron transfer quencher for the luminescence of the QDs. Inset: Energy level diagram corresponding to the electron transfer quenching of the CdSe/ZnS QDs by (**7**). (B) Time-dependent quenching of the luminescence of the QDs upon interaction with the DNA analyte (**8**), 1×10^{-4} M, in the presence of (**7**), 1×10^{-8} M: (a) at $t = 0$ (b) after $t = 1$ h; time-intervals between the recorded curves corresponded to 5 min. Inset: Calibration curve corresponding to the increase of the luminescence of the QDs in the presence of different concentrations of (**8**) after a fixed time interval of 1 h. (C) Analysis of thrombin through the separation of (**7**) from the (**10**)/(**11**) duplex DNA associated with the QDs through the formation of the aptamer-thrombin complex. (D) Time-dependent luminescene increase upon interaction of the (**7**)/(**10**)/(**11**) structure with thrombin, 10 nM. The time interval between recorded curves corresponded to 4 min. Inset: Calibration curve corresponding to the luminescence quenching of the QDs in the presence of different concentrations of thrombin after a fixed time interval of 30 min. (E) Analysis of telomerase by following the hybridization of nucleic acid units complementary to the elongated telomere repeat units, by the intercalation of (**7**) into the resulting duplex structure, resulting in the quenching of the luminescence of the QDs. Reprinted with permission from ref 91. Copyright 2011 Elsevier.

thrombin complex that revealed enhanced stability. The separation of the blocked duplex structure releases the intercalated doxorubicin, thus triggering-on the luminescence of the QDs, Figure 4D. This method enabled the analysis of thrombin with a detection limit corresponding to 10 nM. A further application of the doxorubicin-stimulated electron transfer quenching of the CdSe/ZnS QDs was demonstrated with the analysis of telomerase originating from 293T cancer cell extracts,[91] Figure 4E. According to this method, the primer, (**12**), was elongated by the telomerase in the presence of the dNTPs mixture, to yield the telomere chains consisting of the constant repeat units. The hybridization of nucleic acid sequences (**13**) complementary to the telomere repeat units, and the subsequent intercalation of doxorubicin into the resulting duplex structures, led to the quenching of the luminescence of the QDs. The method enabled the analysis of telomerase that originated from 269 cells/μL.

A further general QD-based sensing platform involving electron transfer quenching relies on the discovery that the hemin/G-quadruplex nanostructure quenches the luminescence of CdSe/ZnS QDs via an electron transfer mechanism,[92] Figure 5A). Accordingly, a DNA sensor was designed by the immobilization of a hairpin structure (**14**) on CdSe/ZnS QDs, Figure 5B. This hairpin structure includes a recognition

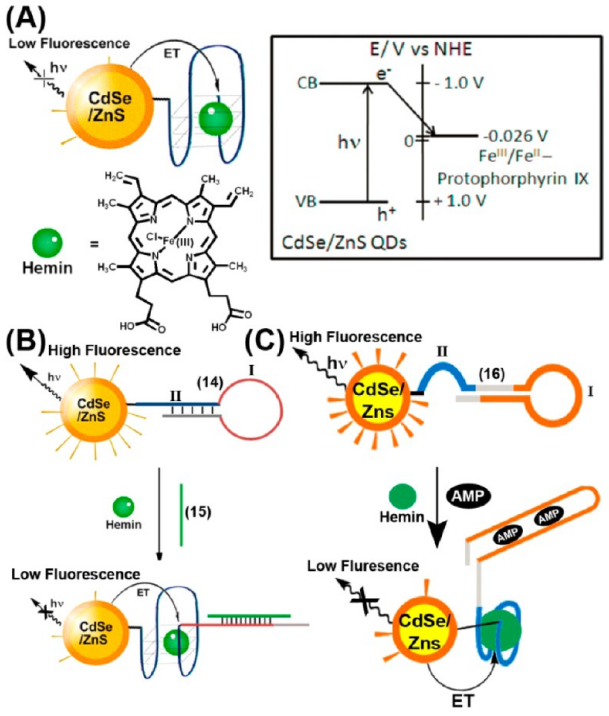

Figure 5. (A) Electron transfer quenching of the luminescence of CdSe/ZnS QDs by the hemin/G-quadruplex. Inset: The appropriate energy levels diagram of the components associated with the electron transfer quenching mechanism. (B) Optical sensing of DNA by a hairpin-modified QDs. Opening of the hairpin by the target leads to self-assembly of the hemin/G-quadruplex that quenches the luminescence of the QDs through an ET process. (C) Optical sensing of AMP by the CdSe/ZnS QDs modified with the hemin/G-quadruplex-aptamer hairpin nanostructure. Adapted with permission from ref 92. Copyright 2010 American Chemical Society.

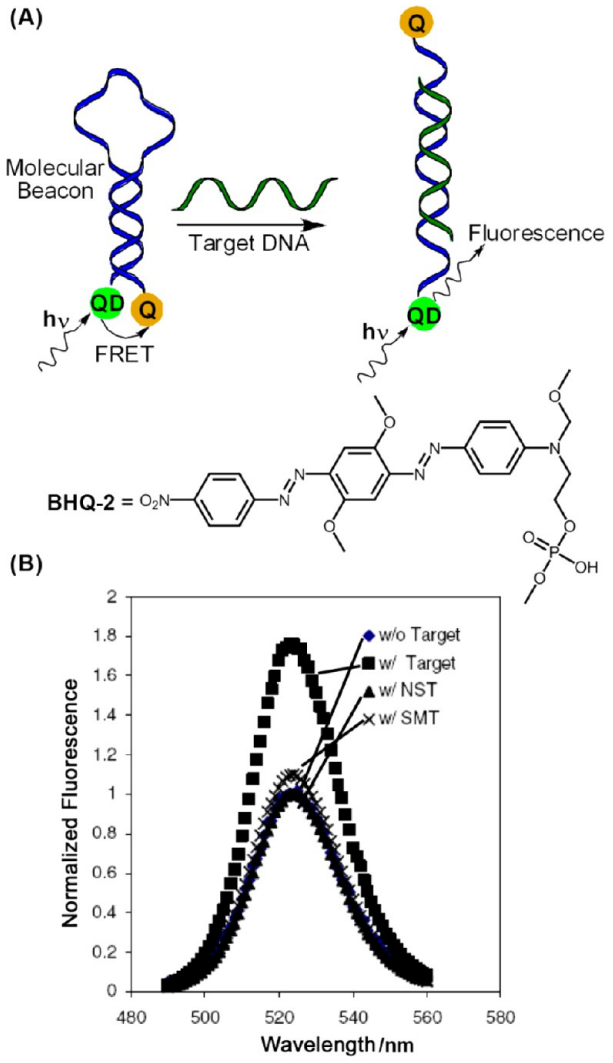

Figure 6. (A) DNA molecular beacon functionalized with QD and quencher units. Opening of the beacon by hybridization of the target turns-on the fluoresence of the QDs. (B) Fluoresence intensities: ♦ without target DNA, ■ with target DNA, ▲ noncomplementary target DNA (NST), × single-base mismatched target DNA (SMT). Reprinted with permission from ref 94. Copyright 2007 IOP Publishing.

sequence (I) for the target DNA, and the G-quadruplex sequence (II), in a caged configuration in the stem region. In the presence of the target, (**15**), the hairpin structure opens, while assembling the hemin/G-quadruplex quencher. As the surface coverage of the QDs by the hemin/G-quadruplex quencher units is controlled by the concentration of the target DNA, the luminescence quenching of the QDs provides a quantitative readout signal for the concentration of the target DNA (detection limit 10×10^{-12} M). This method was further extended to develop an aptamer sensor configuration. This was exemplified with the CdSe/ZnS QDs analysis of adenosine monophosphate, AMP, Figure 5C. A hairpin structure (**16**) composed of the AMP aptamer recognition sequence (region I) and a caged G-quadruplex sequence (II) was linked to the CdSe/ZnS QDs. The AMP-stimulated opening of the hairpin through the formation of the AMP-aptamer complex resulted in the self-organization of the hemin/G-quadruplex nanostructures, leading to the electron transfer quenching of the QDs.

Fluorescence resonance energy transfer (FRET) provides a general mechanism for the detection of DNA. Molecular beacon (MB) nanostructures were functionalized at their ends with CdSe/ZnS QDs and quencher units, respectively, Figure 6A. The steric proximity between the QDs and the quencher units led to the effective quenching of the luminescence of the QDs. The loop region of the hairpin structure of the MB included the recognition sequence for the target. In the presence of the analyte DNA, hybridization of the target to the loop region opened the hairpin structure, resulting in the spatial separation of the QDs from the quencher units, leading to the triggering-on of the luminescence of the QDs.[93−95] For example, the CdSe/ZnS QDs linked to the 5′-end of the hairpin structure were quenched by BHQ-2 acid linked to the 3′-end of the nanostructure, and the assembly was used to analyze a target DNA and to detect single-base mismatches,[93] Figure 6B. Similarly, different sized QDs were used to bind three different hairpin probes for analyzing three different DNA targets. By the functionalization of all hairpins with a versatile black hole quencher (BHQ-2), the luminescence of all QDs was quenched. In the presence of the specific analytes, the targeted selective opening of the respective hairpin occurred, leading to the switching-on of the luminescence of the respective QDs, thus demonstrating the multiplexed analysis of DNAs by the different sized QDs.[94]

A related FRET-based DNA detection scheme has implemented two probe subunits (**17**) and (**18**), complementary to the target DNA (**19**), where probe (**17**) was functionalized with CdSe/ZnS QDs and probe (**18**) was

modified with the Cy5-dye acceptor,[96] Figure 7A. The two probes being separated in solution do not lead to a FRET

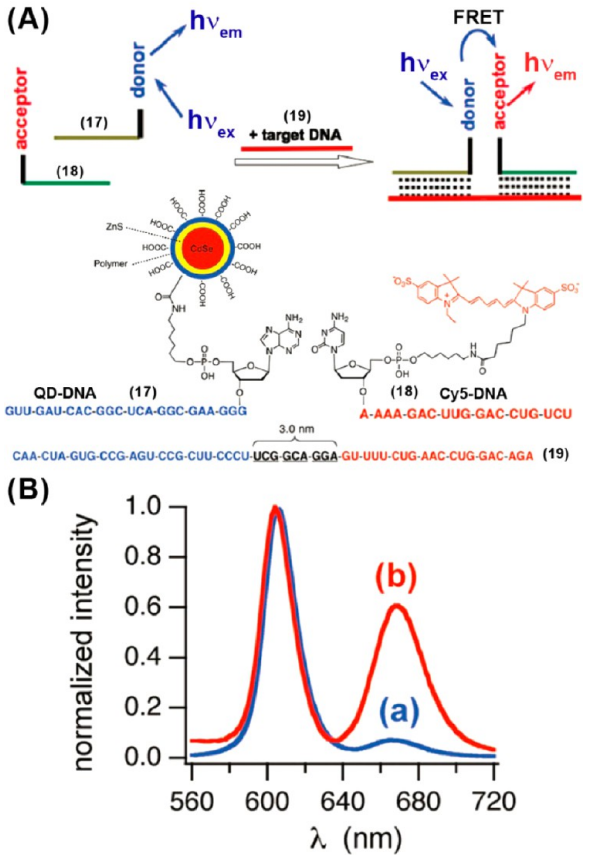

Figure 7. (A) Sensing of a target DNA by hybridizing to two probe DNA strands modified, one with a QD donor and the other with a FRET acceptor, resulting in the FRET process. (B) Normalized fluorescence spectra of the (**17**)-modified QDs, 0.2 μM, Cy5-modified (**18**), 5 μM, (a) prior to the interaction with the target DNA (**19**). (b) After treatment of the components (**17**) and (**18**) with the target DNA (**19**), 5×10^{-6} M. Reproduced with permission from ref 96. Copyright 2012 (Royal Society of Chemistry).

signal, but in the presence of the analyte. The hybridization of the two probes with the DNA analyte, however, yield a tricomponent complex with spatial proximity between the QDs and the Cy5 dye, thus leading to an effective FRET signal, Figure 7B.

A different QD-based DNA sensing platform has implemented a FRET-cascade as readout mechanism,[97] Figure 8A. The system consists of negatively charged carboxylic acid-functionalized CdTe QDs, the positively charged fluorescent conjugated polymer, poly [9,9-bis(N,N-bimethyl)-N-ethylammonium propyl), 2,7-fluorene-1,4-phenylene dibromide, PDFD, (**20**) and the IRD-700-functionalized nucleic acid, (**21**), that is complementary to the target DNA (**22**). The PDFD polymer coats the negatively charged QDs via electrostatic interactions. In the presence of the analyte DNA, the duplex generated between the IRD 700-functionalized probe and the target, binds to the PDFD/CdTe QDs hybrid, resulting in a functional nanostructure that leads to a FRET cascade that reports on the formation of the duplex between the analyte and the IRD-700 reporter nucleic acid, Figure 8B. In this system, the primary FRET process (FRET 1) involves

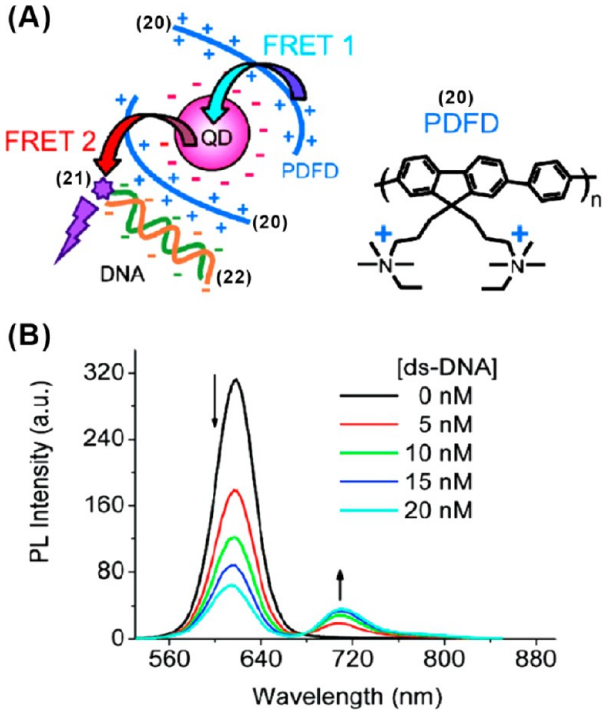

Figure 8. (A) Analysis of DNA by a two-step cascaded FRET using negatively charged QDs coated by the positively charged PDFD polymer chromophore that binds electrostaticly the dye-labled nucleic acid that hybridized with the target. (B) Fluoresence spectra observed upon analysis of different concentrations of the target DNA by the QDs/PDFD hybrid and the dye-functionalized nucleic acid as reporter. Reprinted with permission from ref 97. Copyright 2009 American Chemical Society.

energy transfer from PDFD to the QDs. The internally excited QDs stimulate then the secondary FRET process (FRET 2) to the IRD dye that emits at λ = 720 nm. This FRET cascade enabled the analysis of the analyte DNA with a detection limit corresponding to 1 nM.[97]

An interesting, recently reported, FRET-based analysis of DNA made use of the fact that the single-stranded DNA binds to graphene oxide layers, whereas duplex DNA structures lack affinity for the graphene oxide.[98−101] Accordingly, CdTe QDs were functionalized with a nucleic acid probe (**23**) that is complementary to the target DNA (**24**). In the absence of the target, the QDs bind to the surface of the graphene oxide, leading to the luminescence FRET quenching of the QDs by the graphene oxide, Figure 9A. In the presence of the analyte, formation of the duplex on the QDs prohibits the association of the probe-functionalized QDs to the graphene oxide matrices, thus leading to the triggered-on luminescence of the QDs. As the formation of the duplex structure on the QDs is controlled by the concentration of the target DNA, the resulting luminescence relates to the concentration of the analyte DNA,[102] Figure 9B.

The FRET mechanism was also implemented to detect the formation of aptamer−substrate complexes by means of QDs probes. One approach has involved the modification of the QDs with the aptamer sequence (**25**) and its blocking by a complementary nucleic acid modified with a FRET quencher unit,[103] (**26**), Figure 10A. Formation of the blocked aptamer duplex resulted in the quenching of the luminescence of the QDs. In the presence of the aptamer substrate, however, the duplex separates, while forming the energetically stabilized

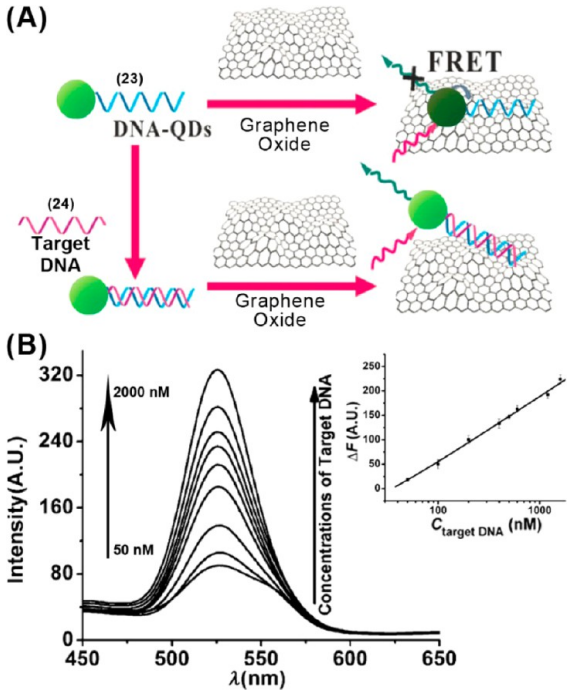

Figure 9. (A) Detection of a target DNA (**24**) using probe-functionalized QDs and graphene oxide as FRET quencher. (B) Fluorescence spectra of the (**23**)-modified QDs after interaction of the QD-functionalized graphene oxide with different concentrations of the target DNA (**24**). Inset: Calibration curve corresponding to the fluorescence increase of the QDs in the presence of different concentrations of the target DNA. Reproduced with permission from ref 102. Copyright 2012 Wiley–VCH.

aptamer–substrate complex. This process removes the quencher units from the QDs, thus triggering-on the luminescence of the QDs. This approach was successfully applied to detect thrombin with a detection limit corresponding to 10 nM.[103] A different method to follow the formation of aptamer–substrate complexes included the application of the "split aptamer" approach, Figure 10(B). According to this method, the aptamer is divided into two subunits (**27**) and (**28**). ALthough one subunit is attached to the QDs (CdSe/ZnS), the other subunit was modified with the FRET dye acceptor. In the presence of the analyte, the subunits assemble into the aptamer-analyte complex, leading to the FRET from the QDs to the fluorophore acceptor and to the fluorescence signal of the dye acceptor. This method was successfully implemented to analyze cocaine, Figure 10(C), with a detection limit that corresponded to 1×10^{-6} M.[104]

The use of a duplex specific intercalating dye that acts as FRET acceptor from photoexcited QDs was, also, implemented to follow the formation of aptamer–substrate complexes. This has been exemplified with the sensing of thrombin using BOBO-3 (**29**) as FRET acceptor from CdSe QDs,[105] Figure 10D. The 565 nm emitting QDs were functionalized with a hairpin DNA (**30**) that acts as probe for analyzing thrombin. The single-stranded loop region of the hairpin includes the aptamer sequence for binding the thrombin analyte, while the stem duplex domain intercalates BOBO-3. In the absence of the analyte, the FRET process from the QDs to BOBO-3 proceeds, leading to the quenching of the luminescence of the QDs and the activation of the fluorescence of BOBO-3. Opening of the hairpin structure through the formation of the aptamer/

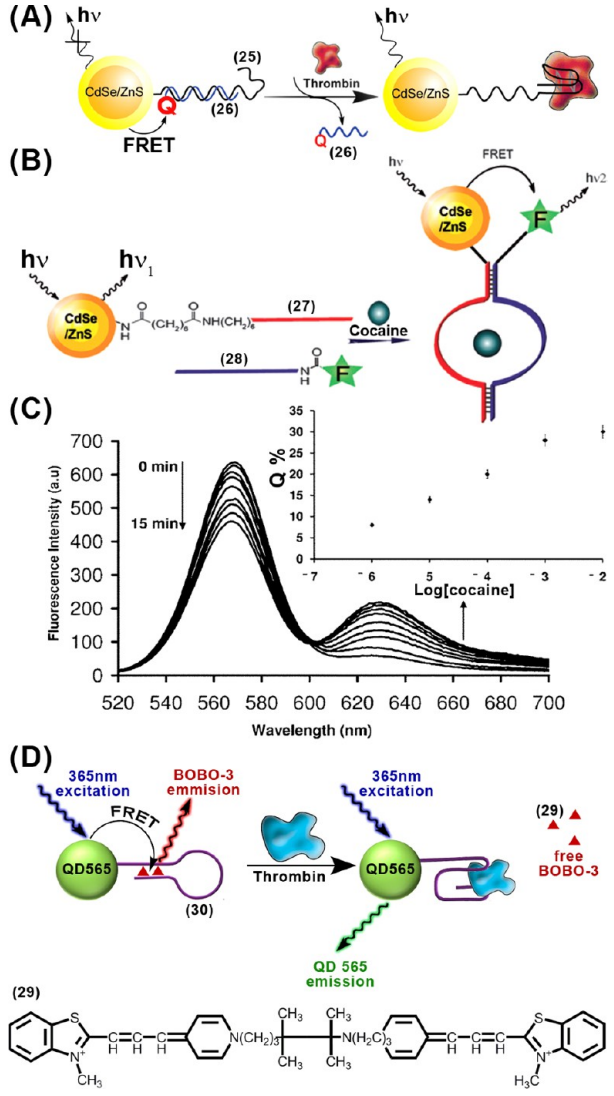

Figure 10. (A) Optical analysis of thrombin by the formation of the aptamer–thrombin complex and the separation of the quencher-nucleic acid blocking unit. (B) Analysis of cocaine by QD/dye aptamer subunits and the implementation of the FRET mechanism. (C) Time-dependent FRET spectra corresponding to the dynamics of the self-assembly of the cocaine-aptamer. Inset: Calibration curve corresponding to the luminescence quenching degree of the QDs by different concentrations of cocaine. (D) Detection of thrombin using a caged-aptamer hairpin modified-QDs and the DNA intercalator BOBO-3. Thrombin binding induces the formation of the aptamer-thrombin complex, leading to the opening of the hairpin and to the release of the BOBO-3 dye units, resulting in the increase of the luminescence of the QDs. B and C are reproduced with permission from ref 104. Copyright 2009 Royal Society of Chemistry. D is reprinted with permission from ref 105. Copyright 2011 Elsevier.

thrombin complex separates the duplex region of the stem, thus leading to the dissociation of BOBO-3. This process eliminates the FRET process, whereas triggering-on the luminescence of the QDs.

A closely related photophysical mechanism for the development of sensors and aptasensors has involved the chemiluminescence resonance energy transfer (CRET) process. This mechanism involves the transfer of chemically generated chemiluminescence energy to the QDs, resulting in the photoexcitation of the QDs and their radiative luminescence

dx.doi.org/10.1021/am303189h | ACS Appl. Mater. Interfaces 2013, 5, 2815–2834

as a result of the electron−hole recombination. This method made use of the fact that the hemin/G-quadruplex acts as a horseradish peroxidase-mimicking catalytic nucleic acid, DNAzyme, that catalyzes the oxidation of luminol by H_2O_2, with the concomitant generation of chemiluminescence.[86,87,106,107] Accordingly, the hemin/G-quadruplex was covalently linked to the CdSe/ZnS QDs,[108] Figure 11A. The chemiluminescence generated by the hemin/G-quadruplex DNAzyme stimulated the CRET process reflected by the activation of the luminescence of the QDs at, λ = 620 nm, Figure 11B. This DNAzyme-stimulated CRET process was then implemented to develop a DNA sensing platform, Figure 11C. The CdSe/ZnS QDs were functionalized with a nanoengineered hairpin structure, (**31**), that included, in its single-stranded loop region, the recognition sequence for the analyte, (**32**), and in its duplex stem region the G-quadruplex sequence in a "caged" inactive configuration. In the presence of the analyte, (**32**), the hairpin structure was opened, resulting in the self-organization of the hemin/G-quadruplex. The DNAzyme-stimulated CRET process to the QDs resulted in the luminescence of the QDs. As the analyte concentration controls the content of the chemiluminescence-generating DNAzyme units, the resulting CRET signal of the QDs relates to the concentration of the analyte, Figure 11D. This method enabled the analysis of DNA with a detection limit corresponding to 10 nM. The advantage of this sensing platform is reflected by a very low background signal, since the luminescence of the QDs is activated only upon opening the probe hairpin structure, a process that generates the internal radiation source for the photoexcitation of the QDs.

This method was further developed for the multiplexed parallel analysis of several DNA targets,[108] Figure 12A. The analytical platform made use of the size-controlled luminescence of the QDs (quantum size effect). Accordingly, three different sized CdSe/ZnS emitting at 490, 560, and 620 nm were functionalized with different hairpin nanostructures (**31**), (**33**), and (**34**). These hairpins included in their single-stranded loop regions the specific recognition sequences complementary to the three target DNAs, (**32**), (**35**), and (**36**), while all hairpin structures included in their stem region the G-quadruplex sequence in an inactive "caged" configuration. In the presence of the respective DNA analytes, the target hairpins were opened, resulting in the self-organization of the hemin/G-quadruplex DNAzyme structure, and the selective activation of the CRET process on which the opening of the hairpin occurred, Figure 12B. By this method, and using the mixture of different sized QDs functionalized with the different hairpin structures, the multiplexed analysis of the different DNAs was demonstrated.[108]

The hemin/G-quadruplex DNAzyme-stimulated CRET process to the QDs was further implemented to develop a new QD-based aptasensor paradigm,[108] Figure 13(A). The anti-ATP aptamer was cleaved into two aptamer subunits (**37**) and (**38**) that were further elongated each by the hemin/G-quadruplex subunit sequences. The 3′-end of subunit (**37**) was covalently linked to CdSe/ZnS QDs. While in the absence of ATP the subunits (**37**) and (**38**) are separated, in the presence of ATP the subunits form the respective aptamer-subunits/ATP complex that is cooperatively stabilized by the hemin/G-quadruplex conjugated to the two aptamer subunits. The hemin/G-quadruplex-catalyzed generation of chemiluminescence triggered-on the CRET process to the QDs, resulting in the luminescence of the QDs. This method enabled the analysis of ATP with a detection limit that corresponded to 1.25×10^{-7} M.[108] Many aptamer sequences adopt a G-

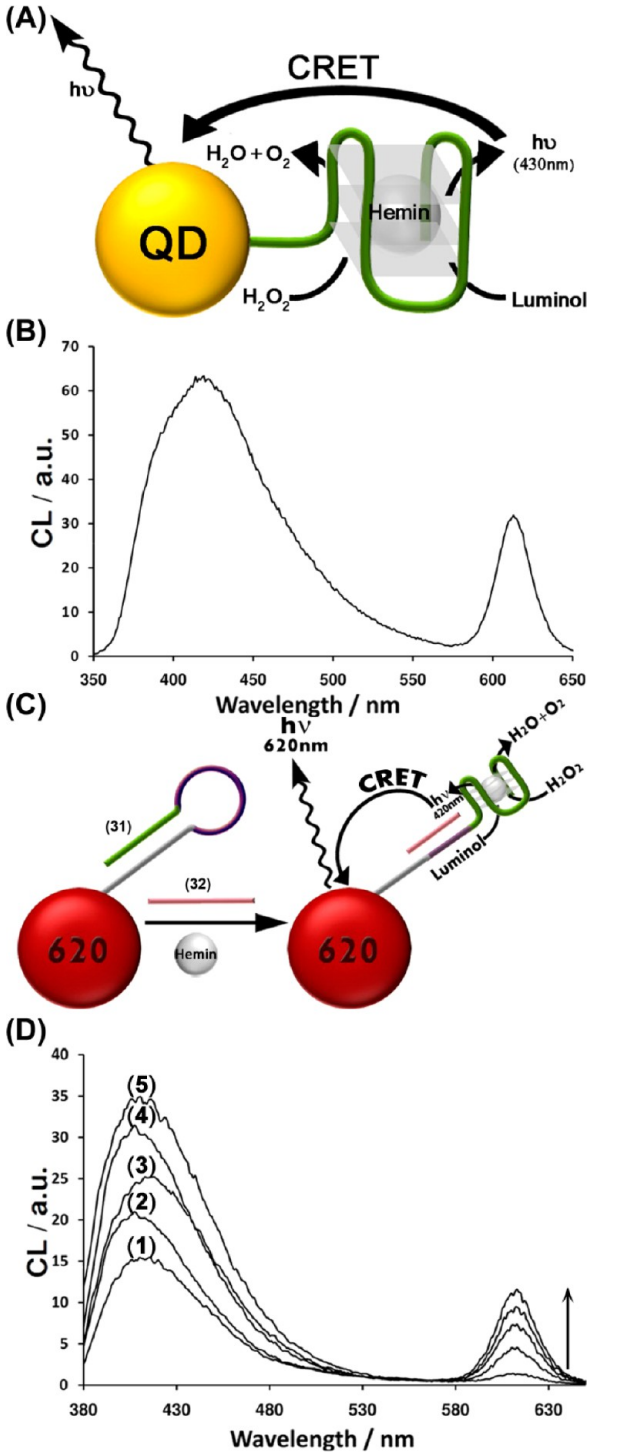

Figure 11. (A) Chemiluminescence resonance energy transfer (CRET) stimulated within the hemin/G-quadruplex QDs hybrid nanostructure in the presence of luminol/H_2O_2. (B) Luminescence spectra corresponding to the CRET signal of the QDs. (C) Analysis of a target DNA by the CRET process from luminol/H_2O_2 to the QDs, by the assembled hemin-G-quadruplex catalyst. (D) Luminescence spectrum corresponding to the CRET signal of the QDs in the absence of (**32**), curve (1), and in the presence of (**32**): (2) 10, (3) 25, (4) 50, and (5) 100 nM. Reprinted with permission from ref 108. Copyright 2011 American Chemical Society.

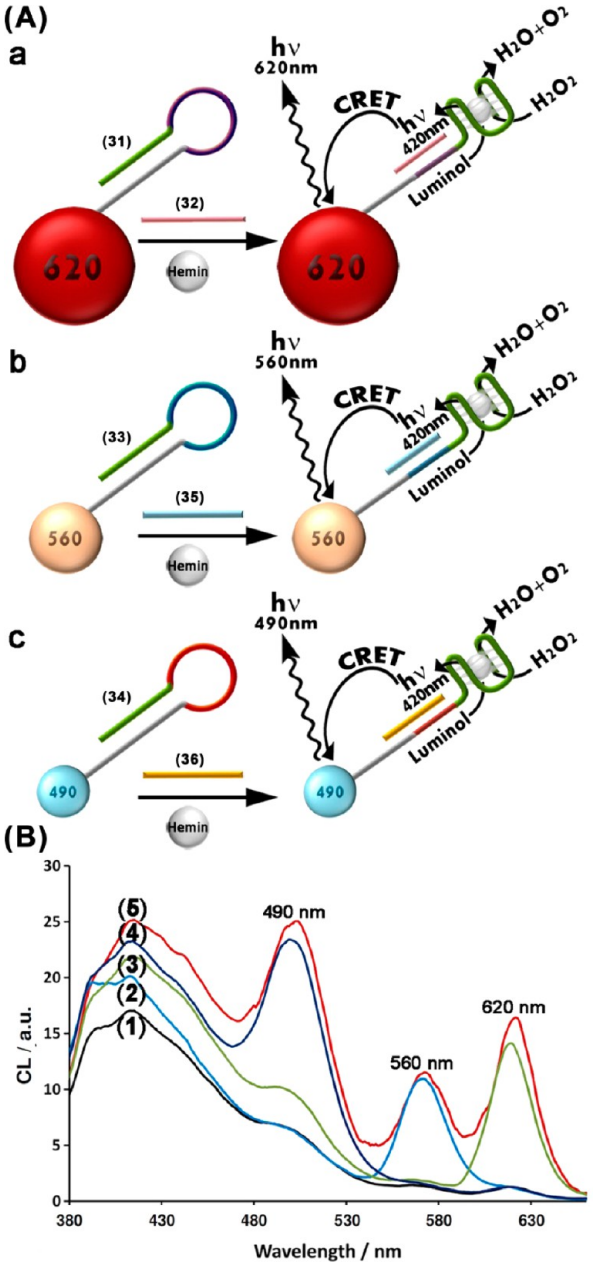

Figure 12. (A) Multiplexed analysis of three different target DNAs based on the CRET sensing scheme using three different sized QDs emitting at: (a) λ = 620 nm, (b) λ = 560 nm, (c) λ = 490 nm. (B) The luminescence spectra corresponding to the CRET luminescence signals of the QDs mixture: (1) in the absence of the different DNA targets, (2) in the presence of (**35**), (3) in the presence of (**32**), (4) in the presence of (**36**), (5) in the presence of all three targets, (**32**), (**35**), and (**36**). Reprinted with permission from ref 108. Copyright 2011 American Chemical Society.

quadruplex structure upon the formation of the aptamer–substrate complex.[109,110] Thus, the labeling of the aptamer with a QD and the implementation of the resulting G-quadruplex as a host nanostructure for hemin, could yield a functional nanoreactor that generates the CRET process as transduction signal for the analysis of the specific substrate. This has been demonstrated with the optical analysis of the Vascular Endothelial Growth Factor (VEGF), Figure 13B. The VEGF describes a family of proteins of different molecular masses that result from alternative gene splicing of the VEGF gene. The

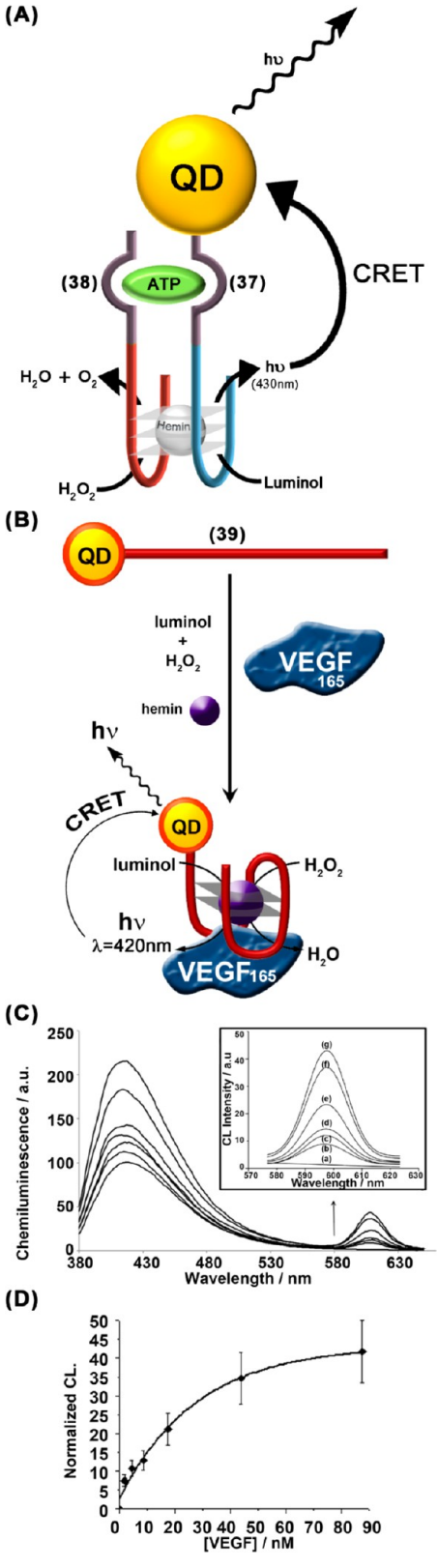

Figure 13. (A) Analysis of ATP through the hemin/G-quadruplex-stimulated generation of chemiluminescence and the CRET-induced generation of luminescence of the QDs. (B) Analysis of $VEGF_{165}$ by the aptamer-modified QDs through the folding of the aptamer into a hemin/G-quadruplex catalytic nanostructure upon the formation of the aptamer/$VEGF_{165}$ complex. The resulting catalyzed generation of chemiluminescence triggers-on the luminescence of the QDs. (C) Luminescence spectra corresponding to the chemiluminescence signal

Figure 13. continued

of the luminol and the CRET signal of the QDs. Inset: The CRET luminescence signals of the QDs in the absence of $VEGF_{165}$, curve (a), and in the presence of different concentrations of $VEGF_{165}$: (b) 8.75×10^{-10} M, (c) 1.75×10^{-9} M, (d) 8.75×10^{-9} M, (e) 1.4×10^{-8} M, (f) 1.75×10^{-8} M, and (g) 8.75×10^{-8} M. A is reprinted with permission from ref 108. (D) The resulting calibration curve. Copyright 2011 American Chemical Society. B–D are reprinted with permission from ref 117. Copyright 2012 American Chemical Society.

major expressed monomer variants are composed of 121, 145, 165, 189, and 206 amino acids.[111] The VEGF growth factor is an important regulator of angiogenesis by activating the VEGF-receptor tyrosine kinase in endothelial cells.[111,112] VEGF induces early embryogenesis through vasulogenesis (blood vessel formation) and angiogenesis (extension of existing blood vessels).[113] The overexpression or down regulation of VEGF are associated with various diseases, such as cancer, neurological disorders, brain injuries, Parkinson's disease, Alzheimer's disease, diabetes mellitus, and psoriasis,[114−116] and therefore is an important biomarker. CdSe/ZnS were functionalized with the anti-$VEGF_{165}$ aptamer (**39**). In the presence of $VEGF_{165}$ the aptamer folded into the G-quadruplex while binding to $VEGF_{165}$. The resulting G-quadruplex provided a host nanostructure for the association of hemin, and the resulting hemin/G-quadruplex catalyzed the generation of chemiluminescence and the subsequent activation of the luminescence of the QDs by the CRET process, Figure 13C. The resulting calibration curve depicting the CRET-stimulated luminescence intensities at variable concentrations of VEGF is shown in Figure 13D. This sensing platform enabled the analysis of $VEGF_{165}$ with a detection limit that corresponded to 8.75×10^{-10} M.[117]

2.2. QDs/Metal NPs/Nucleic Acid (NA) Nanostructures for Optical Sensing. The mechanisms of quenching of semiconductor QDs by metallic nanoparticles (NPs) attracted substantial experimental and theoretical research efforts.[118,119] Specifically, the quenching of the QDs may proceed by an electron transfer route or a resonance energy transfer path, depending on the composition and size of the metallic NPs.[120−123] By the conjugation of nucleic acids to the QDs/metal NPs nanostructure, functional hybrid systems for sensing applications were developed.

The quenching of the luminescence of a nucleic acid-functionalized QDs upon the formation of a duplex structure with the complementary nucleic acid-functionalized Au NPs was demonstrated[124,125] and provided the basis for the development of a DNA sensing platform in solution and on surfaces.[124] The addition of the nucleic acid analyte to the hybrid structure composed of the nucleic acid-functionalized QDs hybridized with the complementary nucleic acid-modified Au NPs resulted in the strand displacement and the separation of the duplex QDs/Au NPs structure, Figure 14A. While in the QD/Au NP hybrid the luminescence of the QDs is quenched, the separation of the hybrid by the analyte triggered-on the luminescence of the QDs, Figure 14B.

The quenching of semiconductor QDs by metallic NPs was further implemented to develop optical aptasensors, and for the multiplexed analysis of analytes using different sized QDs.[126,127] Au NPs were modified with a nucleic acid tag, (**40**), and the anti-adenosine monophosphate aptamer sequence conjugated to a tether sequence complementary to the tag, (**41**), was

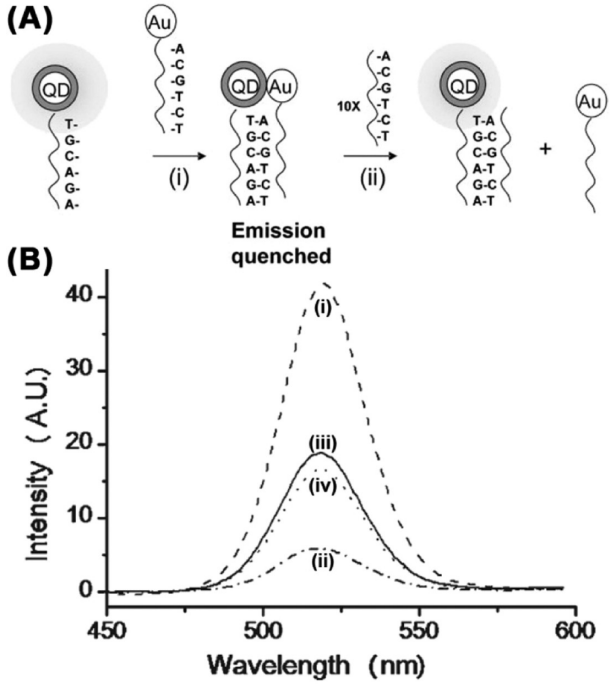

Figure 14. (A) Sensing of a target DNA by a competitive assay using unlabeled and Au-NP-labeled nucleic acid and QDs modified with a complementary nucleic acid. (B) Luminescence spectra corresponding to (i) the luminescence of the nucleic-acid modified QDs; (ii) the luminescence of the nucleic-acid modified QDs in the presence of Au NP-modified nucleic acid; (iii) the luminescence of the nucleic-acid modified QDs in the presence of Au NP-modified nucleic acid and the target DNA; (iv) the luminescence of the nucleic-acid modified QDs in the presence of the target DNA. Reproduced with permission from ref 124. Copyright 2005 Royal Society of Chemistry.

hybridized with the tag nucleic acids linked to Au NPs. The association of the thiolated nucleic acid (**42**)-linked to Au NPs and of the biotinylated nucleic acid (**43**) linked to the QDs through the aptamer chains, resulted in the aggregation of the Au NPs and the conjugated QDs, leading to the quenching of the luminescence of the QDs, Figure 15A. In the presence of the adenosine substrate, the adenosine-aptamer complex releases the QDs from the aggregate, leading to the luminescence of the QDs. By the application of two different sized QDs that include the antiadenosine and anticocaine aptamer sequences, respectively, the multiplexed analysis of the two analytes was demonstrated,[126] Figure 15B.

Also, composite QDs/Au NPs/nucleic acid hybrids were used for the analysis of Hg^{2+} ions. CdSe/ZnS QDs were modified with the nucleic acid (**44**), and Au nanoparticles were functionalized with the nucleic acid (**45**).[128] The nucleic acids (**44**) and (**45**) exhibit partial complementarity and T−T mismatches that prohibit the formation of stable duplexes between the QDs and the Au nanoparticles. In the presence of Hg^{2+} ions, the duplex formation between the strands (**44**) and (**45**) is, however, assisted through the cooperative stabilization by T- Hg^{2+}-T bridges, leading to the aggregation of the QDs and Au nanoparticles, Figure 16A. The fluorescence resonance energy transfer quenching of the QDs by the Au nanoparticles leads to the luminescence decay of the QDs, Figure 16B. This method enabled the selective analysis of Hg^{2+} ions with a detection limit corresponding to 1 nM. The system was successfully applied to analyze Hg^{2+} contaminants in river

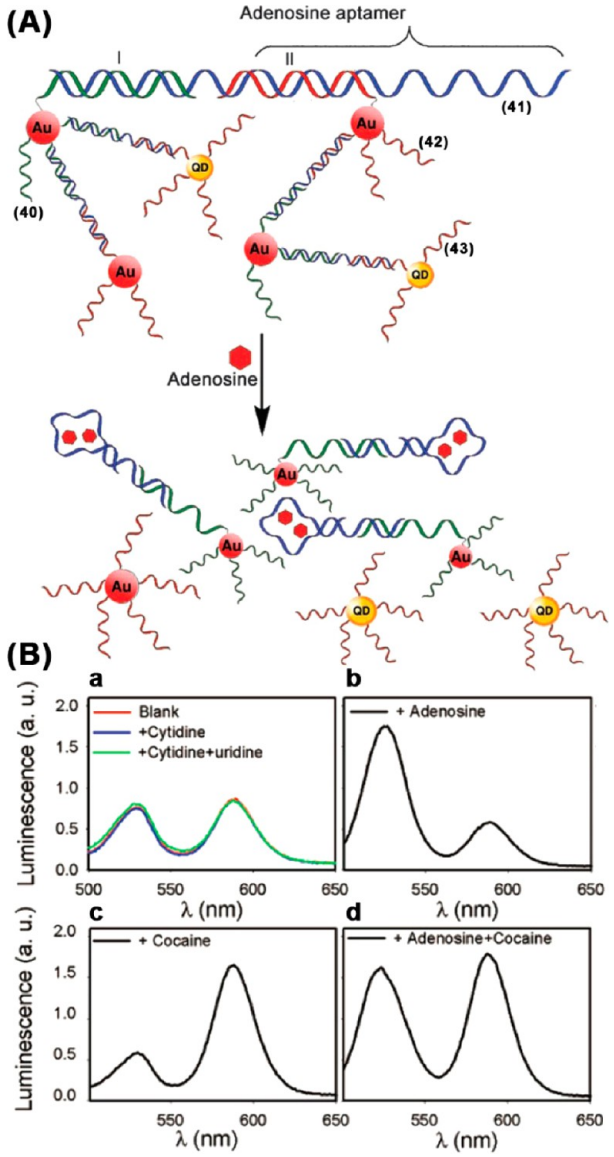

Figure 15. (A) Analysis of adenosine monophosphate (AMP) by fluorescence quenching of Au NPs modified with the functionalized QDs by gold nanoparticles. The anti-adenosine monophosphate aptamer (**41**) bridges the CdSe QD functionalized with nucleic acid (**43**) and the nucleic acid (**40**) to form the respective aggregate. Upon analysis of AMP, the aggregate is separated, and the fluorescence of the QDs is switched on. (B) The fluorescence spectra corresponding to the multiplexed analysis of adenosine and cocaine: (a) in the absence of adenosine and cocaine, or in the presence of 1 mM citidine, or 1 mM cytidine and 1 mM uridine; (b) in the presence of 1 mM adenosine; (c) in the presence of 1 mM cocaine; (d) in the presence of 1 mM adenosine and 1 mM cocaine. Reprinted with permission from ref 126. Copyright 2007 American Chemical Society.

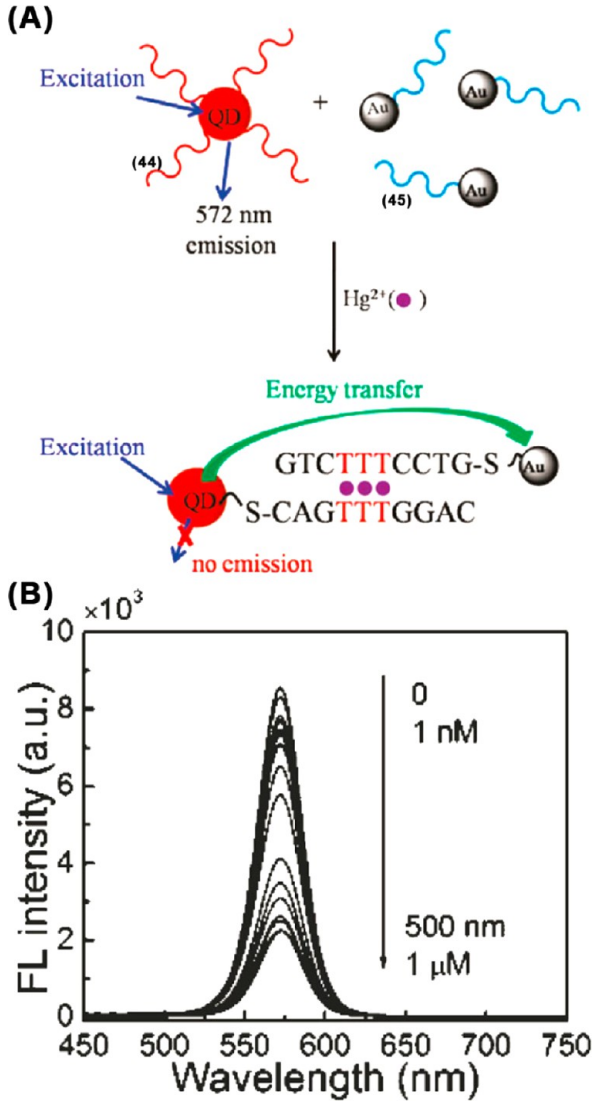

Figure 16. (A) Sensing of Hg^{2+} ions by the T−Hg^{2+}−T-assisted aggregation of the nucleic acids-modified QDs and Au nanoparticles. (B) Fluorescence spectra corresponding to the QDs/Au NPs/nucleic acid hybrids in the presence of different concentrations of Hg^{2+} ions: (0, 1, 2, 3, 4, 5, 6, 8, 10, 15, 20, 30, 40, 60, 80, 100, 200, 500, and 1000 nM). Reprinted with permission from ref 128. Copyright 2011 American Chemical Society.

water[128] (For other QD-based sensing platforms of ions, see section 3).

2.3. Amplified DNA Sensors and Aptasensors. The amplification of sensing events is a fundamental challenge in the development of sensing devices. The fact that semiconductor QDs are each functionalized with many probes consisting of nucleic acids suggests that by the successive regeneration of the target, many of the probes could be utilized in the sensing process, thus leading to participation of many recognition events, rather than single recognition events between the probe and the target DNA. This is exemplified in Figure 17A with the amplified detection of a target DNA through the Exonuclease III, Exo III, biocatalyzed regeneration of the analyte DNA.[129] The CdSe/ZnS QDs are functionalized with the probe nucleic acid, (**46**), modified at its 3′-end with the black-hole quencher, BHQ-2. In this configuration, the luminescence of the QDs is quenched. In the presence of the analyte DNA (**47**) a duplex structure of full complementarity between the 3′ and 5′-ends of (**46**) and (**47**) is formed, whereas the probe is designed in such a way that the 3′-end of the target (**47**) yields a single-stranded nucleic acid overhang that is not recognized by the probe. As Exo III is a "digestive" cleavage biocatalyst that cleaves off the 3′-end nucleobases associated with a duplex DNA, the probe strand in the duplex structure (**46**)/(**47**) is cleaved, leading to the successive removal of the quencher units BHQ-2 and the bases associated with (**46**). The digestion of the probe bases associated with the duplex (**46**)/(**47**) leads to the separation of

dx.doi.org/10.1021/am303189h | ACS Appl. Mater. Interfaces 2013, 5, 2815−2834

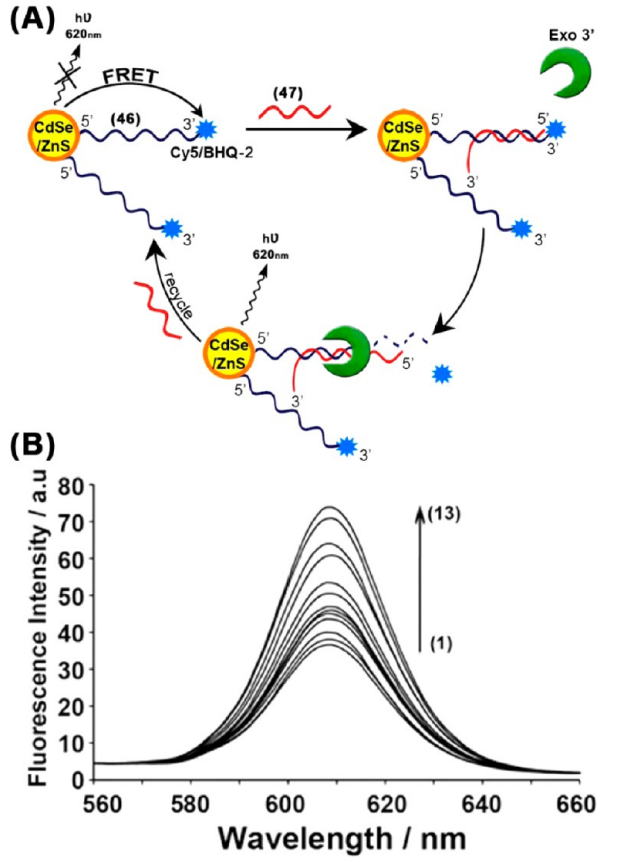

Figure 17. (A) Amplified QD-based sensing of a target DNA by the Exonuclease III-stimulated recycling of the analyte. (B) Time-dependent luminescence spectra of the (**46**)-modified QDs in the absence of the target (**47**), curve (1), and in the presence of (**47**), 1 nM. Spectra were recorded at time intervals of 10 min. Reprinted with permission from ref 129. Copyright 2011 American Chemical Society.

the analyte that binds to another probe unit which, in turn, undergoes the Exo III-catalyzed regeneration of the analyte. As a result, the recognition event between the probe and the analyte triggers-on, in the presence of Exo III, the cyclic regeneration of the analyte. This leads to the amplified detection of the analyte through the regeneration of the analyte and the removal of many quencher units by the regenerated target, Figure 17B. This method enabled the analysis of the target DNA with a detection limit that corresponded to 1×10^{-12} M. The Exo III-catalyzed recycling of the target DNA was, then, implemented for the multiplexed analysis of two different DNAs, Figure 18A. Two different sized QDs emitting at λ_{em} = 620 nm and λ_{em} = 540 nm were modified with the probe nucleic acids (**46**) and (**48**), that are each tethered to the BHQ-2 and BHQ-1 black-hole quenchers, respectively, leading to the quenching of the luminescence of the two types of QDs. These nucleic acids are complementary to the target DNAs (**47**) and (**49**), respectively. Accordingly, the Exo III amplified detection of (**47**), was demonstrated by the 620 nm emitting QDs, Figure 18B, image (a), whereas in the presence of Exo III, amplified sensing of (**49**) was achieved by the 540 nm emitting QDs, Figure 18B (image b). In the presence of the two targets (**47**) and (**49**) and Exo III, the two-sized QDs are triggered-on, Figure 18B, image (c), leading to the luminescence of the two kinds of QDs, thus demonstrating the amplified multiplexed selective analysis of the two targets.[129]

The Exo III-amplified detection of aptamer–substrate complexes was also implemented to analyze the vascular endothelial growth factor (VEGF) (for the significance of this biomarker see section 2.1). The amplified analysis of the $VEGF_{165}$, using the Exo III and the regeneration of the $VEGF_{165}$ analyte, was demonstrated using the "split" aptamer approach,[117] Figure 19A. One subunit of the anti-$VEGF_{165}$ aptamer subunit, (**50**), was functionalized at its 5′-end with CdSe/ZnS QDs, and at the 3′-end, it was modified with the BHQ quencher. This configuration leads to the quenching of the luminescence of the QDs. The second subunit, (**51**), is partially complementary to the subunit (**50**), and thus, in the presence of the target $VEGF_{165}$ analyte, the respective $VEGF_{165}$/aptamer subunits complex is formed, and this is cooperatively stabilized by the duplex region generated between the 3′ and 5′-ends of (**50**) and (**51**), respectively. The formation of the $VEGF_{165}$/aptamer subunits complex in the presence of Exo III leads to the digestive cleavage of the 3′ end of (**50**) at the duplex region associated with (**50**), resulting in the removal of the quencher unit and the separation and regeneration of the $VEGF_{165}$ analyte for a secondary sensing cycle. The autonomous regeneration of the analyte, and the removal of the quencher units, triggered-on the luminescence of the QDs, Figure 19B. This method enabled the amplified analysis of $VEGF_{165}$ with a detection limit corresponding to 5 pM, Figure 19C. This method was successfully implemented to analyze $VEGF_{165}$ in plasma samples, detection limit 50 pm.[117]

2.4. QDs/Nucleic Acid Hybrids for the Analysis of Metal Ions. Nucleobases form complexes with specific metal ions. For example, thymine bases form T-Hg^{2+}-T complexes and cytosine yields C–Ag^{+}–C complexes.[78,79] Also, non-native bases are known to form selective complexes with different metal ions.[130−133] Such metal-ion bridges might cooperatively stabilize the formation of duplex DNA structures. Thus, the generation of metal ion-assisted complexes on QDs might allow the assembly of functional DNA/QDs hybrids for sensing of metal ions. Furthermore, many sequence-specific nucleic acids were found to exhibit catalytic properties in the presence of specific metal ions, such as Mg^{2+}, Cu^{2+}, Pb^{2+}, Hg^{2+}, Zn^{2+}, and more.[134,135] Accordingly, the coupling of metal ion-triggered functional catalytic nucleic acids (DNAzymes) to semiconductor QDs might lead to the design of new metal ion sensing platforms. Also, by the implementation of different sized QDs coupled to the nucleic acid probes that interact with different ions or different sized QDs conjugated to different metal ion-dependent DNAzymes, the multiplexed analysis of metal ions might be achieved.

The optical detection of Hg^{2+} or Ag^{+} ions by nucleic acid-functionalized QDs was demonstrated,[136] Figure 20(A). CdSe/ZnS QDs (λ_{em} = 560 nm) were modified with the thymine-rich nucleic acid, (**52**), whereas larger CdSe/ZnS QDs, (λ_{em} = 620 nm), were functionalized with the cytosine-rich nucleic acid (**53**). In the presence of Hg^{2+} ions, the (**52**)-nucleic acid strand folds into a loop duplex structure stabilized by T–Hg^{2+}–T bridges, leading to the selective quenching of the luminescence of the (**52**)-modified QDs. Similarly, treatment of the (**53**)-functionalized QDs with Ag^{+} ions resulted in the folding of the C-rich nucleic acids (**53**) to form C–Ag^{+}–C stabilized duplex structures, leading to the selective quenching of the luminescence of the (**53**)-modified QDs, Figures 20B and C.

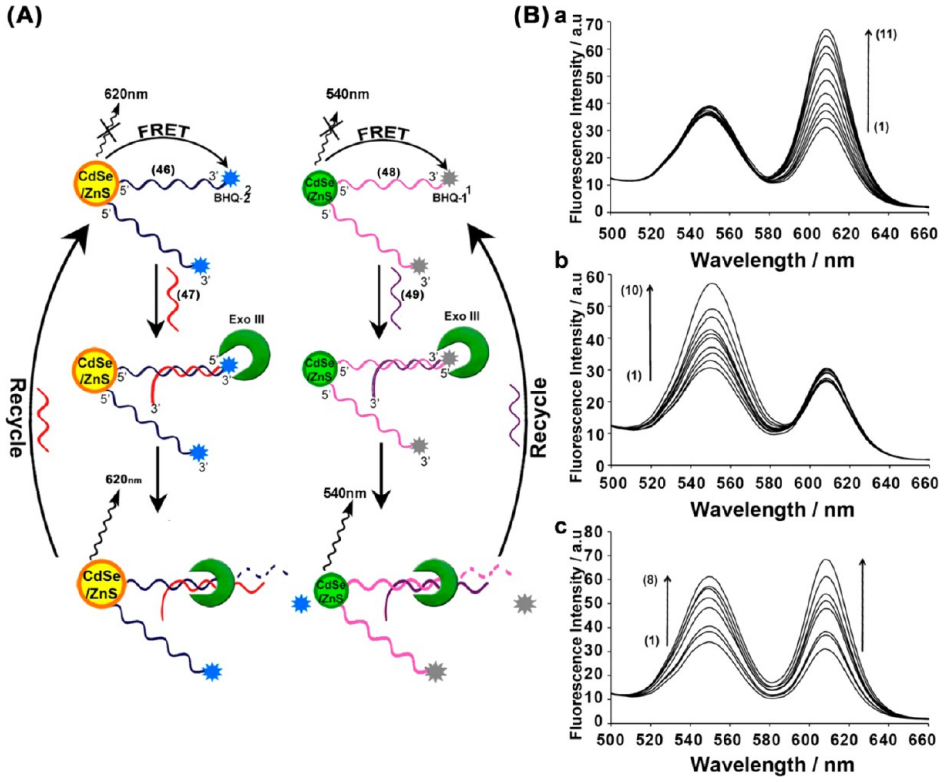

Figure 18. (A) Amplified multiplexed analysis of different target nucleic acids, (**47**) and (**49**), by the probe modified 620 nm and 540 nm emitting QDs, respectively, using the Exo III-catalyzed digestion and the target recycling scheme. (B) Time-dependent luminescence spectra corresponding to the amplified multiplexed analysis of the target DNAs, (**47**) and (**49**): (a) in the presence of (**47**), 1 nM, taken at time intervals of 10 min; (b) in the presence of (**49**), 1 nM, taken at time intervals of 12 min; (c) in the presence of both (**47**) and (**49**), 1 nM, taken at time intervals of 15 min. Reprinted with permission from ref 129. Copyright 2011 American Chemical Society.

Upon mixing the two sized QDs, the multiplexed analysis of Hg^{2+} and Ag^{+} was demonstrated, Figure 20D.[136]

The QD-based analysis of metal ions using metal-dependent DNAzymes was demonstrated with the selective analysis of Pb^{2+} and Cu^{2+},[137] Figure 21(A). CdSe/ZnS QDs emitting at 625 or 530 nm were protected by a SiO_2 shell, and the QDs were functionalized with the ribonucleobase-containing nucleic acids, (**54**) and (**55**), respectively. The nucleic acid (**54**), attached to the 625 nm QDs, includes the substrate sequence of the Cu^{2+}-dependent DNAzyme, whereas the nucleic acid, (**55**), associated with the 530 nm emitting QDs, is composed of the substrate sequence corresponding to the Pb^{2+}-dependent DNAzyme. The sequence-specific Cu^{2+}-dependent DNAzyme (**54**), and Pb^{2+}-dependent DNAzyme, (**55**), were functionalized, similarly, with quencher units, and hybridized with the respective substrates associated with the QDs. In the presence of Cu^{2+} ions or Pb^{2+} ions, the DNAzymes cleave-off the respective substrates, resulting in the triggering-on of the luminescence of the 625 and 530 nm QDs, respectively. The time-dependent integrated luminescence intensities provided then the readout signals for the quantitative detection of Cu^{2+} or Pb^{2+} ions, respectively, Figure 21B.

3. NUCLEIC ACIDS/QDS CONJUGATES FOR PHOTOELECTROCHEMICAL SENSING

Photoexcitation of semiconductor QDs yields the formation of an electron−hole pair in the conduction-band and valence-band of the QDs. Coupling of the photoexcited QDs to electrode supports may then trigger electron transfer reactions between the QDs and the electrode, resulting in the generation of photocurrents. Controlling these electron transfer reactions by means of biological processes allows, then, the probing of biotransformations through the photoelectrochemical function of the QDs.[138,139]

The photoelectrochemical transduction of biorecognition events is presented with the analysis of cocaine using a CdS QD-functionalized aptasensor electrode.[140] The "split" aptamer approach was implemented to develop the bioanalytical assay, Figure 22A. The aptamer against cocaine was split into two subunits. The thiolated aptamer subunit, (**56**), was linked to the electrode, and the second aptamer subunit (**57**) was used to modify the QDs. In the presence of cocaine, the cocaine/aptamer subunits were formed on the electrode surface. Photoexcitation of the QDs resulted in the ejection of the conduction-band electrons to the electrode, and to the concomitant oxidation of the triethanolamine, TEOA, by valence-bond holes, leading to a steady-state anodic photocurrent. As the surface coverage of the electrode is controlled by the concentration of cocaine, the resulting photocurrent provides a quantitative signal for the content of the analyte, Figure 23B.

The successful implementation of the hemin/G-quadruplex-catalyzed generation of chemiluminescence (in the presence of H_2O_2/luminol), and the secondary chemiluminescence resonance energy transfer (CRET)-stimulated excitation of semiconductor QDs, was used to develop photoelectrochemical sensing platforms without external irradiation.[141] CdS QDs were immobilized on Au electrodes and capped with bovine serum albumin (BSA). The enzyme glucose oxidase, GOx, modified with hemin/G-quadruplex units was covalently linked

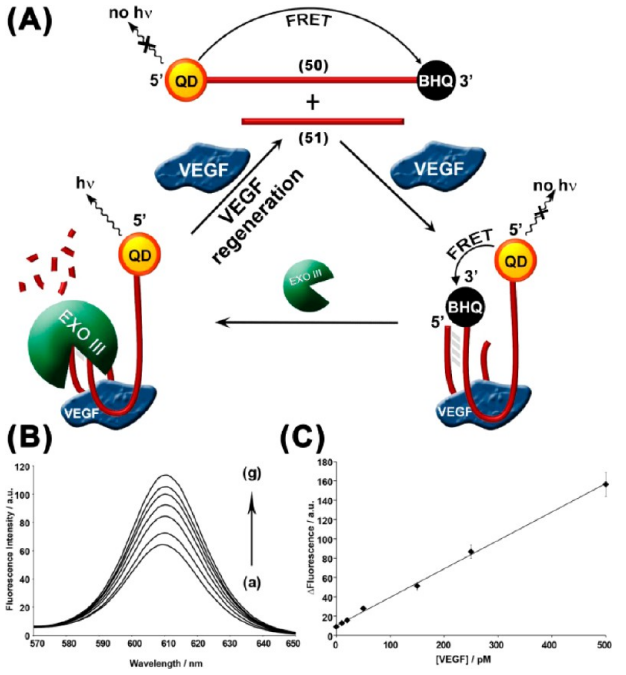

Figure 19. (A) Amplified fluorescence sensing of $VEGF_{165}$ using two aptamer subunits (**50**) and (**51**), and Exo III-catalyzed regeneration of $VEGF_{165}$. (B) Time-dependent luminescence spectra of the (**50**)-modified QDs: curve (a), in the absence of $VEGF_{165}$; curves (b−g) in the presence of 150 pM $VEGF_{165}$, taken at time intervals of 15 min. (C) Calibration curve corresponding to the resulting increase of the fluorescence of the (**50**)-modified QDs upon interaction with different concentrations of $VEGF_{165}$ for a fixed time interval of 90 min. Reprinted with permission from ref 117. Copyright 2012 American Chemical Society.

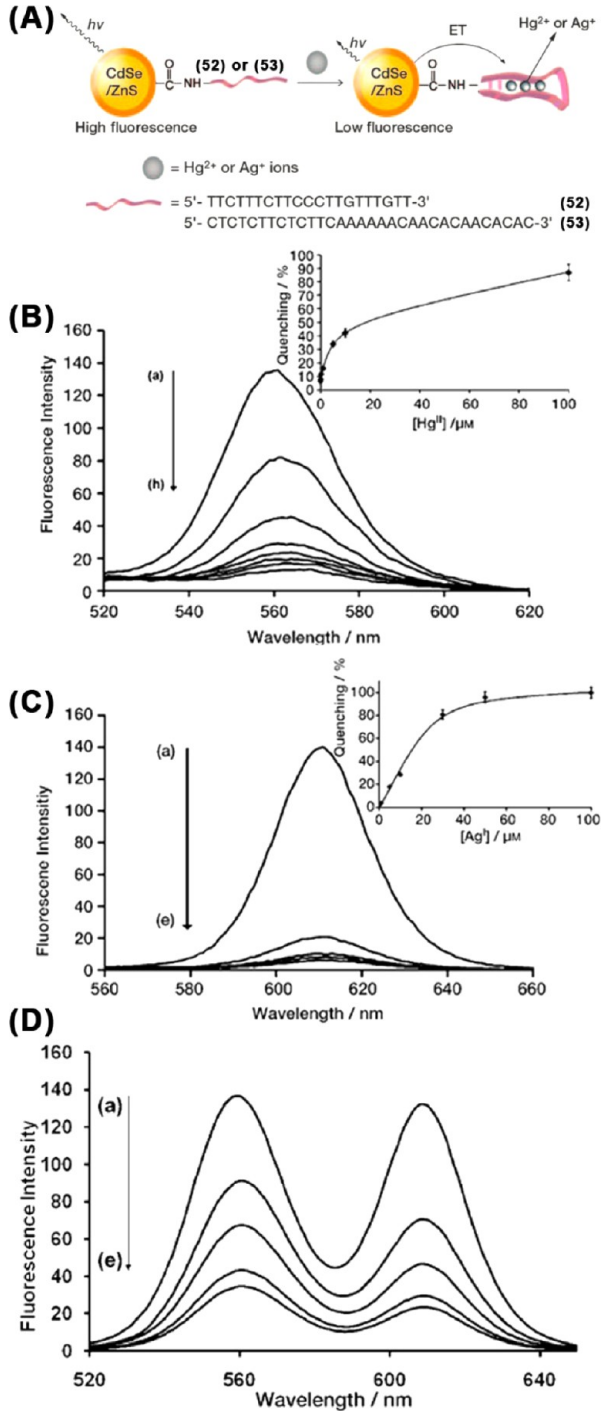

Figure 20. (A) Optical analysis of Hg^{2+}/Ag^{+} ions by nucleic acid-modified QDs. (B) Time-dependent luminescence spectra of the (**52**)-QD560 upon interaction with 1×10^{-4} M Hg^{2+}. Inset: Calibration curve for various concentrations of Hg^{2+}. (C) Time-dependent luminescence spectra of the (**53**)-QD620 upon interaction with 5×10^{-5} M Ag^{+}. Inset: Calibration curve for various concentrations of Ag^{+}. (D) Fluorescence changes of the (**52**)-QD560 and (**53**)-QD620 upon interaction with: a) no Hg^{2+}, no Ag^{+}; b)-e) upon interaction with Hg^{2+} and Ag^{+}, 10, 20, 30, and 50 μM, respectively. Spectra recorded after a fixed time interval of 30 min. Reproduced with permission from ref 136. Copyright 2009 Wiley−VCH.

to the CdS QDs, Figure 23A. The GOx-catalyzed oxidation of glucose yields gluconic acid and H_2O_2, and the latter product acts as a cosubstrate for the hemin/G-quadruplex generation of chemiluminescence in the presence of luminol. The resulting chemiluminescence activates the CRET process to the QDs, resulting in the generation of the photocurrent. The photocurrent is generated by ejection of the conduction-band electrons to the electrode, and the concomitant scavenging of the valence-band holes by the supply of electrons from the solution-solubilized electron donor, triethanolamine, TEOA. As the generated chemiluminescence is controlled by the concentration of glucose, the resulting photocurrents relate to the concentration of glucose, Figure 23B. Similarly, the photoelectrochemical detection of DNA, without external irradiation, was demonstrated using the CRET process as internal light source, Figure 23C. A probe nucleic acid, (**58**), complementary to a part of the target-analyte DNA, (**59**), was covalently linked to the CdS QDs associated with an electrode. The hemin/G-quadruplex catalytic label was conjugated to a nucleic acid chain, (**60**), that was complementary to the single-stranded domain of the analyte, that formed the recognition complex (**59**)/(**60**) on the electrode. The DNAzyme-catalyzed generation of chemiluminescence by the hemin/G-quadruplex in the "sandwich-type" CdS QDs/DNA/hemin/G-quadruplex structure stimulated then the CRET process and the formation of the photocurrent. As the surface coverage of the DNAzyme is controlled by the concentration of the analyte DNA, (**59**), the resulting chemiluminescence intensities, and consequently, the magnitude of photocurrent, related to the concentration of the target DNA, Figure 23D. The method enabled the detection of the DNA with a detection limit corresponding to 1 nM. The photoelectrochemical CRET-stimulated analysis

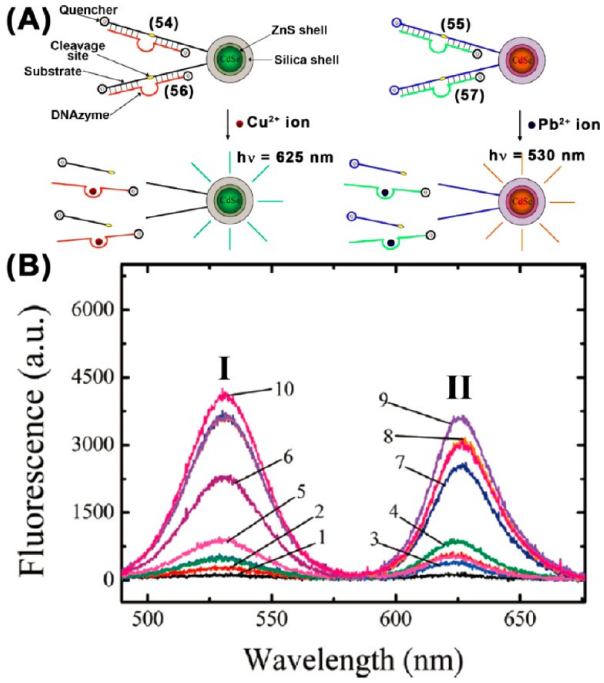

Figure 21. (A) Schematic multiplexed detection of metal ions using DNAzyme-functionalized different sized CdSe/ZnS QDs. (B) (I) Fluorescence spectra of the QDs–DNAzyme conjugates after interaction with various concentrations of Pb^{2+} ions, taken after a fixed time interval of 25 min. (II) Fluorescence spectra of the QDs–DNAzyme conjugates after interaction with various concentrations of Cu^{2+} ions, taken after a fixed time-interval of 25 min. Reprinted with permission from ref 137. Copyright 2010 American Chemical Society.

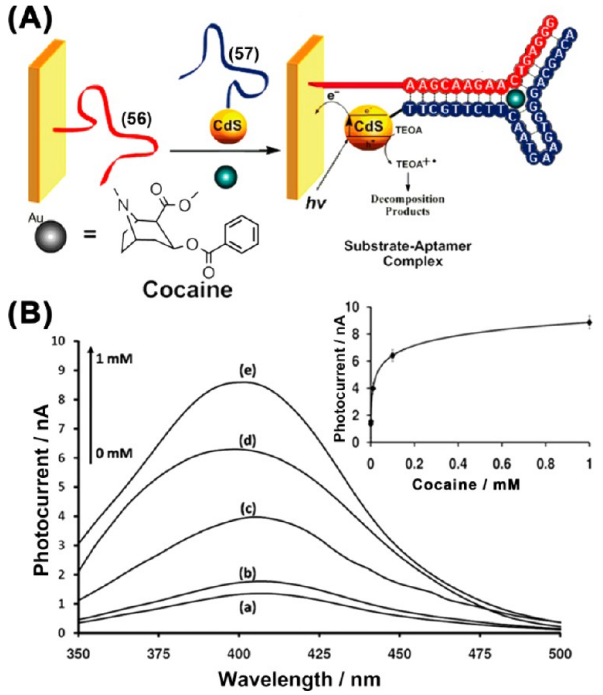

Figure 22. (A) Photoelectrochemical cocaine sensor based on the self-organization of cocaine/aptamer subunits complex on an Au electrode. (B) Photocurrent action spectra corresponding to the analysis of different concentrations of cocaine by the functionalized electrode: (a) in the absence of cocaine; (b) in the presence of 1 μM, (c) 10 μM, (d) 100 μM, (e) 1 mM. Reprinted with permission from ref 140. Copyright 2009 American Chemical Society.

of glucose or of DNA represents a unique method to develop photoelectrochemical biosensor devices that generate currents, as readout signals, without external irradiation source or electrical power supply.

4. PROBING DNA MACHINES BY NUCLEIC ACID/QDS CONJUGATES

Substantial recent research efforts in the area of DNA nanotechnology are directed toward the development of molecular DNA machines.[77,142−149] By encoding appropriate information in the base sequences of DNA nanostructures, and by the application of appropriate fuel/antifuel substrates, programmed mechanical operations in the nanoengineered nanostructures are activated. Different DNA machines including tweezers,[150,151] walkers,[152,153] gears,[154] cranes,[155] and more[156] were reported. One of the challenges in the development of DNA machines, includes, however, the development of readout signals that probe the states of the machines, and more importantly, the dynamics of the machine operation. The unique photophysical properties of QDs, and their participation in fluorescence resonance energy transfer, chemiluminescence resonance energy transfer, and photoelectrochemical reactions pave the way to introduce new QD-based readout methods for DNA machines.

CdSe/ZnS QDs were implemented to follow the reversible "walking" process of a DNA using adenosine monophosphate, AMP, as fuel,[157] Figure 24. The nucleic acid strand (**61**) was linked to the QDs, and it acted as a scaffold for the hybridization of two footholds (**62**) and (**63**). The foothold (**62**) includes the AMP-aptamer sequence. The nucleic acid

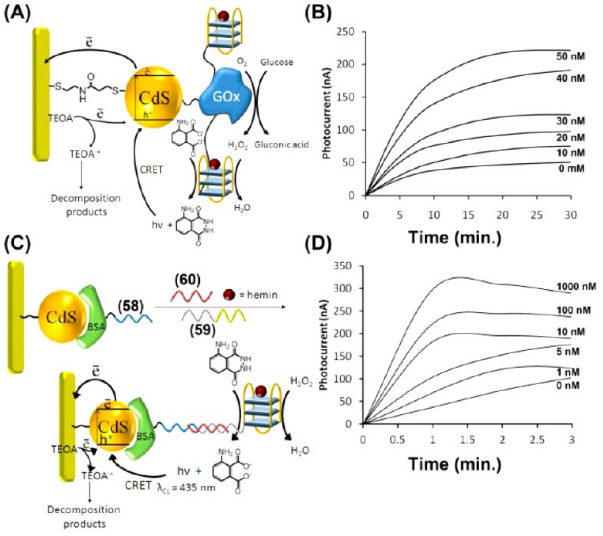

Figure 23. (A) Analysis of glucose by the glucose oxidase/CdS QD-functionalized Au electrode, using the hemin/G-quadruplex as a catalytic label for the CRET-stimulated generation of photocurrents. (B) Time-dependent photocurrents generation upon analyzing different concentrations of glucose by the system shown in panel A. (C) Analysis of a target DNA by a sandwich-type nucleic acid assay on the BSA/CdS QD-functionalized Au electrode, using the hemin/G-quadruplex as a catalytic label for the CRET-stimulated generation of photocurrents. (D) Time-dependent photocurrents generated upon analyzing different concentrations of the target DNA, (**59**), according to the sensing scheme depicted in (C). Reprinted with permission from ref 141. Copyright 2012 American Chemical Society.

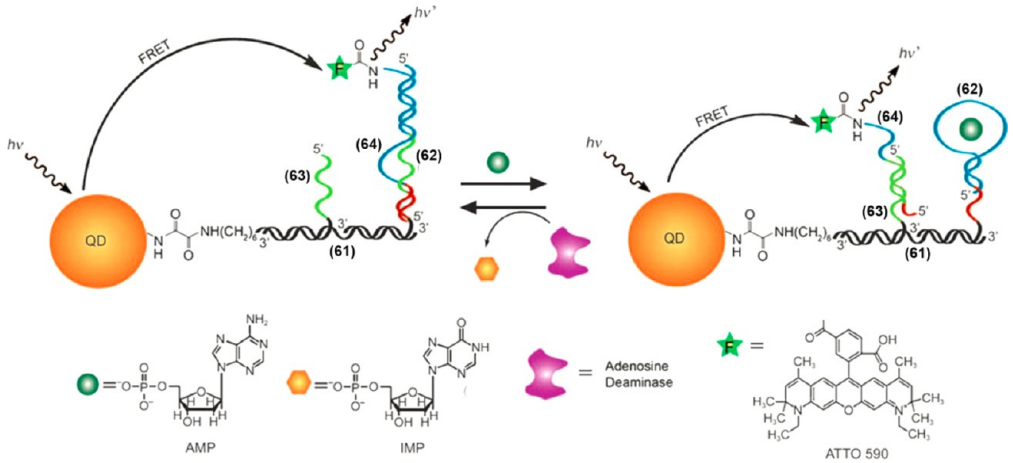

Figure 24. Monitoring the switchable translocation of a dye-labeled nucleic acid on a DNA track, associated with a CdSe/ZnS QD, by fluorescence resonance energy transfer (FRET). Reproduced with permission from ref 157. Copyright 2009 Royal Society of Chemistry.

strand (**64**) included partially complementary sequence that can bind to footholds (**62**) and (**63**), yet the system was designed to form a duplex structure with the aptamer-containing sequence associated with foothold (**62**). In the presence of AMP, the formation of AMP-aptamer complex on foothold (**62**) was energetically favored, leading to the release of (**64**) and its walkover to foothold (**63**). The chemically induced adenosine deaminase-stimulated transformation of AMP to inosine monophosphate, IMP, which lacks affinity for the aptamer sequence, resulted in the separation of the IMP/aptamer complex and the formation of the free foothold (**62**). This initiated, then, the reverse translocation of the walker unit from foothold (**63**) to foothold (**62**) to yield the duplex of enhanced stability. The walking process on the DNA scaffold was monitored by the labeling of the walker element with the ATTO 590 dye, and following the FRET process between the QDs and the dye. The occupation of foothold (**62**) with the walker yielded a high FRET signal due to the proximity between the donor–acceptor units, and lower FRET signals upon binding of the walker to foothold (**63**), because of the spatial separation of the donor–acceptor components. By the cyclic addition of the AMP fuel, and its biocatalyzed degradation by adenosine deaminase, the cyclic translocation of the walker was demonstrated,[157] using the FRET as readout signals.

In a different study,[158] the hemin/G-quadruplex generation of chemiluminescence was used to stimulate the chemiluminescence resonance energy transfer process to semiconductor QDs, as readout signal for the walking process, Figure 25A. The DNA (**65**) was used as scaffold to immobilize, through hybridization, three footholds consisting of the (**66**)-functionalized CdSe/ZnS QDs, the nucleic acid (**67**) that includes a protruding single-strand unit, and a third foothold (**68**) to which the walker element (**69**) is hybridized. The walker includes the G-quadruplex sequence, and is caged in a duplex structure with foothold (**68**), that prohibits the formation of the G-quadruplex. In the presence of the fuel-strand (**70**), displacement of the walker strand (**69**) proceeds, leading to the formation of the duplex (**68**)/(**70**) and the translocation of the walker (**69**) to foothold (**67**), where the G-quadruplex sequence is unblocked and yields a hemin/G-quadruplex catalytic structure. The hemin/G-quadruplex catalyzes the generation of chemiluminescence, and the resulting chemiluminescence resonance energy transfer (CRET) process to the QDs triggers-on the luminescence of the QDs. Subjection of the system to the antifuel strand (**71**) displaces the fuel strand (**70**) from foothold (**67**), resulting in the separation of the duplex (**70**)/(**71**), leading to the reverse translocation of the walker from foothold (**67**) to foothold (**68**) to yield the energetically stabilized nanostructure (**68**)/(**69**). In this configuration, the G-sequence of (**69**) is blocked in a duplex structure that does not yield chemiluminescence. By the reversible treatment of the system with the fuel/antifuel strand, the cyclic bidirectional operation of the walker was demonstrated using the CRET as readout signal, Figure 25B. In a related system,[158] the three footholds/scaffold hybrid structure was assembled on a Au electrode, and the CRET-stimulated generation of the photocurrent was used as readout signal for the bidirectional walking process, Figure 25C. The displacement of the walker (**69**) from foothold (**68**) by the fuel strand, (**70**), leads to the translocation of the walker to foothold (**67**), while generating the catalytically active hemin/G-quadruplex. The resulting chemiluminescence activates the CRET process to the QDs, leading to the excitation of the CdSe/ZnS QDs, and the formation of the electron/hole species. The ejection of the conduction band electrons to the electrode, and the concomitant oxidation of triethanolamine by the valence-band holes, led to the generation of a steady state photocurrent, Figure 25D. This enabled the probing of the bidirectional translocation of the walker on the DNA scaffold associated with the electrode by means of the CRET-induced photocurrent signal.

5. CONCLUSIONS

The present article has summarized recent applications of nucleic acid/semiconductor QD hybrid systems for analytical and DNA nanotechnology applications. The analytical applications of these hybrid nanostructures made use of the unique photophysical properties of the QDs (high luminescence quantum yields, photostability, size-controlled luminescence features), and the functional recognition and catalytic properties encoded in nucleic acid sequences (duplex formation through complementary hybridization, binding of low-molecular-weight substrates or macromolecules to aptamers, catalytic properties of nucleic acids-DNAzymes, and selective binding of ions by nucleotides). Different photophysical mechanisms including fluorescence, electron transfer quenching, fluores-

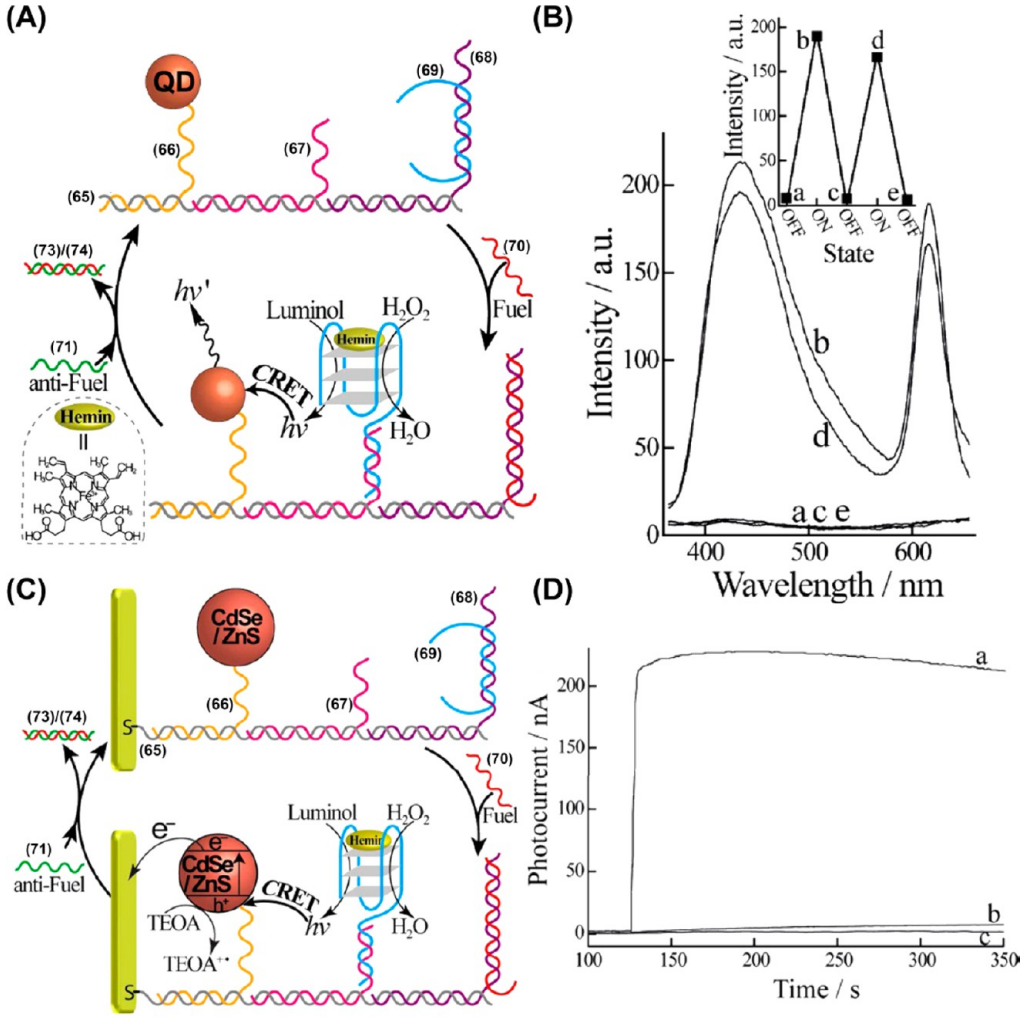

Figure 25. (A) Probing a reversible DNA walker by the switchable formation of the hemin/G-quadruplex DNAzyme and the DNAzyme-stimulated generation of a CRET signal to the CdSe/ZnS QDs. (B) Luminescence spectra corresponding to the QDs system: (a) The walker (**69**) is in foothold (**68**). (b) After the fueled walkover of (**69**) to foothold (**67**).(c) After the reverse translocation of (**69**) to foothold (**68**) using the antifuel strand. (d, e) Second cycle of moving the walker (**69**) to foothold (**67**) and back to foothold (**68**). Inset: the cyclic switchable CRET signals of the walker system. (C) Switchable photoelectrochemical transduction of a DNA "walker" associated on an electrode, using the hemin/G-quadruplex generated chemiluminescence, and the subsequent CRET-induced generation of photocurrent, as a readout signal for the walking process. (D) Time-dependent photocurrents upon: (a) the fueled positioning of the walker (**69**) on foothold (**67**); (b) the antifueled reverse positioning of the walker (**69**) on foothold (**68**); (c) control experiments corresponding to the photocurrent where the CdSe/ZnS QDs are excluded from the scaffold and the DNAzyme (**69**) is positioned on foothold (**67**). Reprinted with permission from ref 158. Copyright 2013 American Chemical Society.

cence resonance energy transfer (FRET) and chemiluminescence resonance energy transfer (CRET) were implemented to develop the different nucleic acid/QD-based sensing platforms. These analytical methods may find important diagnostic applications in the analysis of genetic disorders, tissue matching, detection of pathogens, and more.

The important advances in the use of QDs for analytical applications, however, rest on the size-controlled luminescence properties of QDs. This enables the use of the same chemistry to modify different QDs for detecting different target analytes. Furthermore, the fact that these versatile multiprobe-functionalized QDs can be excited by a common wavelength allows the application of mixtures of different sized QDs for the multiplexed, parallel, detection of different analytes. Indeed, different DNAs corresponding to different pathogens or DNA biomarkers for certain diseases were analyzed, in parallel, by QDs. Similarly, the multiplexed analyses of aptamer-complexes or of metal ions were performed by different sized QDs modified with the appropriate sequence-specific recognition nucleic acids.

The use of nucleic acid/QDs hybrids for the development of photoelectrochemical sensing devices is a particularly novel approach. Specifically, the development of photoelectrochemical sensing devices based on the chemiluminescence resonance energy transfer (CRET) process represent a recent advance where photocurrents are generated, as a result of recognition events, without any external irradiation. Such systems could bridge the boundaries between nucleic acid-based optical and electrochemical sensing platforms.

One important topic in the application of QDs for sensing processes relates to the amplification of the detection platforms. The use of exonuclease III, Exo III, as a biocatalyst for the autonomous regeneration of the target DNA or the aptamer–substrate was demonstrated. One may envisage other biocatalytic processes to regenerate the target DNA, e.g., the application of endonucleases[159] or ligation DNAzymes.[160,161]

The recent sensing platforms that stimulate the autonomous target-induced polymerization of DNAzyme wires[162,163] (e.g., the formation of hemin/G-quadruplex DNAzyme wires) may be coupled to QDs, thus providing new methods for the amplified optical analysis of DNA, aptamer−substrate complexes or ions.

While nucleic acid/QDs hybrids demonstrated their potential impact for bioanalysis, important challenges are still ahead of us. The rapid progress in the application of other functional nanoscale materials for sensing (e.g., graphene, graphene oxide, carbon nanoparticles) and the elucidation of new optical properties of these materials suggest that by coupling the nucleic acid/QDs hybrids with such graphitic carbon nanostructures, new sensing materials and innovative detection platforms could be envisaged. Also, the incorporation of the nucleic acid/QDs hybrids into cells and the in vivo sensing of analytes is a challenging future goal.

AUTHOR INFORMATION

Corresponding Author

*Phone: +972-2-6585272. Fax: +972-2-6527715. E-mail: willnea@vms.huji.ac.il.

Notes

The authors declare no competing financial interest.

ACKNOWLEDGMENTS

This research is supported by the Israel Science Foundation.

REFERENCES

(1) Gaponenko, S. V. *Optical Properties of Semiconductor Nanocrystals*; Cambridge University Press: Cambridge, U.K., 1998.
(2) Valizadeh, A.; Mikaeili, H.; Samiei, M.; Farkhani, S. M.; Zarghami, N.; Kouhi, M.; Akbarzadeh, A.; Davaran, S. *Nanoscale Res. Lett.* **2012**, *7*, 480.
(3) Amelia, M.; Lincheneau, C.; Silvi, S.; Credi, A. *Chem. Soc. Rev.* **2012**, *41*, 57285743.
(4) Gaponenko, S. V. *Semiconductors* **1996**, *30*, 315−336.
(5) Grieve, K.; Mulvaney, P.; Grieser, F. *Curr. Opin. Colloid Interface Sci.* **2000**, *5* (168), 168−172.
(6) Yoffe, A. D. *Adv. Phys.* **2001**, *50*, 1−208.
(7) Murray, C. B.; Norris, D. J.; Bawendi, M. G. *J. Am. Chem. Soc.* **1993**, *115*, 8706−8715.
(8) Peng, Z. A.; Peng, X. G. *J. Am. Chem. Soc.* **2001**, *123*, 183−184.
(9) Qu, L. H.; Peng, Z. A.; Peng, X. G. *Nano Lett.* **2001**, *1*, 333−337.
(10) Qu, L. H.; Peng, X. G. *J. Am. Chem. Soc.* **2002**, *124*, 2049−2055.
(11) Manna, L.; Scher, E. C.; Alivisatos, A. P. *J. Am. Chem. Soc.* **2000**, *122*, 12700−12706.
(12) Milliron, D. J.; Hughes, S. M.; Cui, Y.; Manna, L.; Li, J. B.; Wang, L. W.; Alivisatos, A. P. *Nature* **2004**, *430*, 190−195.
(13) Manna, L.; Milliron, D. J.; Meisel, A.; Scher, E. C.; Alivisatos, A. P. *Nat. Mater.* **2003**, *2*, 382−385.
(14) Wang, D. L.; Lieber, C. M. *Nat. Mater.* **2003**, *2*, 355−356.
(15) Kan, S.; Mokari, T.; Rothenberg, E.; Banin, U. *Nat. Mater.* **2003**, *2*, 155−158.
(16) Yu, J. H.; Joo, J.; Park, H. M.; Baik, S. I.; Kim, Y. W.; Kim, S. C.; Hyeon, T. *J. Am. Chem. Soc.* **2005**, *127*, 5662−5670.
(17) Manna, L.; Scher, E. C.; Li, L. S.; Alivisatos, A. P. *J. Am. Chem. Soc.* **2002**, *124*, 7136−7145.
(18) Pacholski, C.; Kornowski, A.; Weller, H. *Angew. Chem., Int. Ed.* **2002**, *41*, 1188−1191.
(19) Chan, W. C. W.; Nie, S. M. *Science* **1998**, *281*, 2016−2018.
(20) Dubertret, B.; Skourides, P.; Norris, D. J.; Noireaux, V.; Brivanlou, A. H.; Libchaber, A. *Science* **2002**, *298*, 1759−1762.
(21) Jaiswal, J. K.; Mattoussi, H.; Mauro, J. M.; Simon, S. M. *Nat. Biotechnol.* **2003**, *21*, 47−51.
(22) Pathak, S.; Choi, S. K.; Arnheim, N.; Thompson, M. E. *J. Am. Chem. Soc.* **2001**, *123*, 4103−4104.
(23) Querner, C.; Reiss, P.; Bleuse, J.; Pron, A. *J. Am. Chem. Soc.* **2004**, *126*, 11574−11582.
(24) Dubois, F.; Mahler, B.; Dubertret, B.; Doris, E.; Mioskowski, C. *J. Am. Chem. Soc.* **2007**, *129*, 482−483.
(25) Kim, S.; Bawendi, M. G. *J. Am. Chem. Soc.* **2003**, *125*, 14652−14653.
(26) Kim, S. W.; Kim, S.; Tracy, J. B.; Jasanoff, A.; Bawendi, M. G. *J. Am. Chem. Soc.* **2005**, *127*, 4556−4557.
(27) Yang, C.-H.; Bhongale, C. J.; Chou, C.-H.; Yang, S.-H.; Lo, C.-N.; Chen, T.-M.; Hsu, C.-S. *Polymer* **2007**, *48*, 116−128.
(28) Jaffar, S.; Nam, K. T.; Khademhosseini, A.; Xing, J.; Langer, R. S.; Belcher, A. M. *Nano Lett.* **2004**, *4*, 1421−1425.
(29) Schneider, G.; Decher, G. *Nano Lett.* **2004**, *4*, 1833−1839.
(30) Potapova, I.; Mruk, R.; Prehl, S.; Zentel, R.; Basche, T.; Mews, A. *J. Am. Chem. Soc.* **2003**, *125*, 320−321.
(31) Yu, W. W.; Chang, E.; Falkner, J. C.; Zhang, J. Y.; Al-Somali, A. M.; Sayes, C. M.; Johns, J.; Drezek, R.; Colvin, V. L. *J. Am. Chem. Soc.* **2007**, *129*, 2871−2879.
(32) Luccardini, C.; Tribet, C.; Vial, F.; Marchi-Artzner, V.; Dahan, M. *Langmuir* **2006**, *22*, 2304−2310.
(33) Zhang, H.; Cui, Z. C.; Wang, Y.; Zhang, K.; Ji, X. L.; Lu, C. L.; Yang, B.; Gao, M. Y. *Adv. Mater.* **2003**, *15*, 777−780.
(34) Petruska, M. A.; Bartko, A. P.; Klimov, V. I. *J. Am. Chem. Soc.* **2004**, *126*, 714−715.
(35) Anderson, R. E.; Chan, W. C. W. *Acs Nano* **2008**, *2*, 1341−1352.
(36) Kairdolf, B. A.; Mancini, M. C.; Smith, A. M.; Nie, S. *Anal. Chem.* **2008**, *80*, 3029−3034.
(37) Kairdolf, B. A.; Smith, A. M.; Nie, S. *J. Am. Chem. Soc.* **2008**, *130*, 12866−12867.
(38) Pellegrino, T.; Manna, L.; Kudera, S.; Liedl, T.; Koktysh, D.; Rogach, A. L.; Keller, S.; Radler, J.; Natile, G.; Parak, W. J. *Nano Lett.* **2004**, *4*, 703−707.
(39) Di Corato, R.; Quarta, A.; Piacenza, P.; Ragusa, A.; Figuerola, A.; Buonsanti, R.; Cingolani, R.; Manna, L.; Pellegrino, T. *J. Mater. Chem.* **2008**, *18*, 1991−1996.
(40) Mattoussi, H.; Mauro, J. M.; Goldman, E. R.; Anderson, G. P.; Sundar, V. C.; Mikulec, F. V.; Bawendi, M. G. *J. Am. Chem. Soc.* **2000**, *122*, 12142−12150.
(41) Gerion, D.; Pinaud, F.; Williams, S. C.; Parak, W. J.; Zanchet, D.; Weiss, S.; Alivisatos, A. P. *J. Phys. Chem. B* **2001**, *105*, 8861−8871.
(42) Bruchez, M.; Moronne, M.; Gin, P.; Weiss, S.; Alivisatos, A. P. *Science* **1998**, *281*, 2013−2016.
(43) Wu, X. Y.; Liu, H. J.; Liu, J. Q.; Haley, K. N.; Treadway, J. A.; Larson, J. P.; Ge, N. F.; Peale, F.; Bruchez, M. P. *Nat. Biotechnol.* **2003**, *21*, 41−46.
(44) Gao, X. H.; Cui, Y. Y.; Levenson, R. M.; Chung, L. W. K.; Nie, S. M. *Nat. Biotechnol.* **2004**, *22*, 969−976.
(45) Alivisatos, A. P. *Science* **1996**, *271*, 933−937.
(46) Alivisatos, A. P. *J. Phys. Chem.* **1996**, *100*, 13226−13239.
(47) Nirmal, M.; Brus, L. *Acc. Chem. Res.* **1999**, *32*, 407−414.
(48) Kuno, M.; Lee, J. K.; Dabbousi, B. O.; Mikulec, F. V.; Bawendi, M. G. *J. Chem. Phys.* **1997**, *106*, 9869−9882.
(49) Dabbousi, B. O.; Rodriguez-Viejo, J.; Mikulec, F. V.; Heine, J. R.; Mattoussi, H.; Ober, R.; Jensen, K. F.; Bawendi, M. G. *J. Phys. Chem. B* **1997**, *101*, 9463−9475.
(50) Ellingson, R. J.; Beard, M. C.; Johnson, J. C.; Yu, P. R.; Micic, O. I.; Nozik, A. J.; Shabaev, A.; Efros, A. L. *Nano Lett.* **2005**, *5*, 865−871.
(51) Schaller, R. D.; Klimov, V. I. *Phys. Rev. Lett.* **2004**, *92*, 1866011−1866014.
(52) Plass, R.; Pelet, S.; Krueger, J.; Grätzel, M.; Bach, U. *J. Phys. Chem. B* **2002**, *106*, 7578−7580.
(53) Nozik, A. J. *Physica E* **2002**, *14*, 115−120.
(54) Kamat, P. V. *J. Phys. Chem. C* **2007**, *111*, 2834−2860.
(55) Kamat, P. V. *Chem. Rev.* **1993**, *93*, 267−300.
(56) Thompson, T. L.; Yates, J. T. *Top. Catal.* **2005**, *35*, 197−210.
(57) Tachikawa, T.; Fujitsuka, M.; Majima, T. *J. Phys. Chem. C* **2007**, *111*, 5259−5275.

(58) Harris, C.; Kamat, P. V. *Acs Nano* **2009**, *3*, 682−690.
(59) Snee, P. T.; Somers, R. C.; Nair, G.; Zimmer, J. P.; Bawendi, M. G.; Nocera, D. G. *J. Am. Chem. Soc.* **2006**, *128*, 13320−13321.
(60) Walker, G. W.; Sundar, V. C.; Rudzinski, C. M.; Wun, A. W.; Bawendi, M. G.; Nocera, D. G. *Appl. Phys. Lett.* **2003**, *83*, 3555−3557.
(61) Hildebrandt, N. *ACS Nano* **2011**, *5*, 5286−5290.
(62) Medintz, I. L.; Uyeda, H. T.; Goldman, E. R.; Mattoussi, H. *Nat. Mater.* **2005**, *4*, 435−446.
(63) Freeman, R.; Willner, I. *Chem. Soc. Rev.* **2012**, *41*, 4067−4085.
(64) Chan, W. C. W.; Maxwell, D. J.; Gao, X. H.; Bailey, R. E.; Han, M. Y.; Nie, S. M. *Curr. Opin. Biotechnol.* **2002**, *13*, 40−46.
(65) Somers, R. C.; Bawendi, M. G.; Nocera, D. G. *Chem. Soc. Rev.* **2007**, *36*, 579−591.
(66) Gill, R.; Zayats, M.; Willner, I. *Angew. Chem., Int. Ed.* **2008**, *47*, 7602−7625.
(67) Hoetzer, B.; Medintz, I. L.; Hildebrandt, N. *Small* **2012**, *8*, 2297−2326.
(68) Jin, Z.; Hildebrandt, N. *Trends Biotechnol.* **2012**, *30*, 394−403.
(69) Algar, W. R.; Susumu, K.; Delehanty, J. B.; Medintz, I. L. *Anal. Chem.* **2011**, *83*, 8826−8837.
(70) Freeman, R.; Willner, B.; Willner, I. *ACS Symp. Ser.* **2012**, *1112*, 1−31.
(71) Lakowicz, J. R. *Principles of Fluorescence Spectroscopy*, Springer, New York, 2006.
(72) Eaton, B. E.; Gold, L.; Zichi, D. A. *Chem. Biol.* **1995**, *2*, 633−638.
(73) Gold, L.; Polisky, B.; Uhlenbeck, O.; Yarus, M. *Annu. Rev. Biochem.* **1995**, *64*, 763−797.
(74) Cox, J. C.; Hayhurst, A.; Hesselberth, J.; Bayer, T. S.; Georgiou, G.; Ellington, A. D. *Nucleic Acids Res.* **2002**, *30*, e108.
(75) Breaker, R. R. *Nat. Biotechnol.* **1997**, *15*, 427−431.
(76) Lu, Y.; Liu, J. *Curr. Opin. Biotechnol.* **2006**, *17*, 580−588.
(77) Willner, I.; Shlyahovsky, B.; Zayats, M.; Willner, B. *Chem. Soc. Rev.* **2008**, *37*, 1153−1165.
(78) Clever, G. H.; Kaul, C.; Carell, T. *Angew. Chem., Int. Ed.* **2007**, *46*, 6226−6236.
(79) Ono, A.; Cao, S.; Togashi, H.; Tashiro, M.; Fujimoto, T.; Machinami, T.; Oda, S.; Miyake, Y.; Okamoto, I.; Tanaka, Y. *Chem. Commun.* **2008**, 4825−4827.
(80) Li, D.; Wieckowska, A.; Willner, I. *Angew. Chem., Int. Ed.* **2008**, *47*, 3927−3931.
(81) Lee, J.-S.; Han, M. S.; Mirkin, C. A. *Angew. Chem., Int. Ed.* **2007**, *46*, 4093−4096.
(82) Wang, L.-R.; Qu, N.; Guo, L.-H. *Anal. Chem.* **2008**, *80*, 3910−3914.
(83) Wain, A. J.; Zhou, F. *Langmuir* **2008**, *24*, 5155−5160.
(84) Kelley, S. O.; Boon, E. M.; Barton, J. K.; Jackson, N. M.; Hill, M. G. *Nucleic Acids Res.* **1999**, *27*, 4830−4837.
(85) Kelley, S. O.; Barton, J. K.; Jackson, N. M.; Hill, M. G. *Bioconjugate Chem.* **1997**, *8*, 31−37.
(86) Travascio, P.; Li, Y. F.; Sen, D. *Chem. Biol.* **1998**, *5*, 505−517.
(87) Travascio, P.; Witting, P. K.; Mauk, A. G.; Sen, D. *J. Am. Chem. Soc.* **2001**, *123*, 1337−1347.
(88) Gerion, D.; Chen, F. Q.; Kannan, B.; Fu, A. H.; Parak, W. J.; Chen, D. J.; Majumdar, A.; Alivisatos, A. P. *Anal. Chem.* **2003**, *75*, 4766−4772.
(89) Song, W.; Qiu, X.; Lau, C.; Lu, J. *Anal. Chim. Acta* **2012**, *735*, 114−120.
(90) Yuan, J.; Guo, W.; Yang, X.; Wang, E. *Anal. Chem.* **2009**, *81*, 362−368.
(91) Raichlin, S.; Sharon, E.; Freeman, R.; Tzfati, Y.; Willner, I. *Biosens. Bioelectron.* **2011**, *26*, 4681−4689.
(92) Sharon, E.; Freeman, R.; Willner, I. *Anal. Chem.* **2010**, *82*, 7073−7077.
(93) Kim, J. H.; Morikis, D.; Ozkan, M. *Sens. Actuators, B* **2004**, *102*, 315−319.
(94) Kim, J. H.; Chaudhary, S.; Ozkan, M. *Nanotechnology* **2007**, *18*, 195105−195112.
(95) Cady, N. C.; Strickland, A. D.; Batt, C. A. *Mol. Cell. Probes* **2007**, *21*, 116−124.
(96) Peng, Y.; Qiu, C.; Jockusch, S.; Scott, A. M.; Li, Z.; Turro, N. J.; Ju, J. *Photochem. Photobiol. Sci.* **2012**, *11*, 881−884.
(97) Jiang, G.; Susha, A. S.; Lutich, A. A.; D, S. F.; Feldmann, J.; Rogach, A. L. *ACS Nano* **2009**, *3*, 4127−4131.
(98) Liu, Y.; Dong, X.; Chen, P. *Chem. Soc. Rev.* **2012**, *41*, 2283−2307.
(99) Wang, Y.; Li, Z.; Wang, J.; Li, J.; Lin, Y. *Trends Biotechnol.* **2011**, *29*, 205−212.
(100) Lu, C.-H.; Yang, H.-H.; Zhu, C.-L.; Chen, X.; Chen, G.-N. *Angew. Chem., Int. Ed.* **2009**, *48*, 4785−4787.
(101) He, S.; Song, B.; Li, D.; Zhu, C.; Qi, W.; Wen, Y.; Wang, L.; Song, S.; Fang, H.; Fan, C. *Adv. Funct. Mater.* **2010**, *20*, 453−459.
(102) Zhang, C.; Xu, J.; Zhang, S.; Ji, X.; He, Z. *Chem.–Eur. J.* **2012**, *18*, 8296−8300.
(103) Levy, M.; Cater, S. F.; Ellington, A. D. *ChemBioChem* **2005**, *6*, 2163−2166.
(104) Freeman, R.; Li, Y.; Tel-Vered, R.; Sharon, E.; Elbaz, J.; Willner, I. *Analyst* **2009**, *134*, 653−656.
(105) Chi, C.-W.; Lao, Y.-H.; Li, Y.-S.; Chen, L.-C. *Biosens. Bioelectron.* **2011**, *26*, 3346−3352.
(106) Travascio, P.; Bennet, A. J.; Wang, D. Y.; Sen, D. *Chem. Biol.* **1999**, *6*, 779−787.
(107) Witting, P. K.; Travascio, P.; Sen, D.; Mauk, A. G. *Inorg. Chem.* **2001**, *40*, 5017−5023.
(108) Freeman, R.; Liu, X.; Willner, I. *J. Am. Chem. Soc.* **2011**, *133*, 11597−11604.
(109) Li, T.; Wang, E.; Dong, S. *Chem. Commun.* **2008**, 5520−5522.
(110) Li, T.; Shi, L. L.; Wang, E. K.; Dong, S. J. *Chem.–Eur. J.* **2009**, *15*, 1036−1042.
(111) Neufeld, G.; Cohen, T.; Gengrinovitch, S.; Poltorak, Z. *FASEB J.* **1999**, *13*, 9−22.
(112) Ferrara, N. *Endocr. Rev.* **2004**, *25*, 581−611.
(113) Hoeben, A.; Landuyt, B.; Highley, M. S.; Wildiers, H.; Van Oosterom, A. T.; De Bruijn, E. A. *Pharmacol. Rev.* **2004**, *56*, 549−580.
(114) Storkebaum, E.; Lambrechts, D.; Carmeliet, P. *Bioessays* **2004**, *26*, 943−954.
(115) Tarkowski, E.; Issa, R.; Sjogren, M.; Wallin, A.; Blennow, K.; Tarkowski, A.; Kumar, P. Neurobiol. *Aging* **2002**, *23*, 237−243.
(116) Crawshaw, A. A.; Griffiths, C. E. M.; Young, H. S. *Expert Opin. Invest. Drugs* **2012**, *21*, 33−43.
(117) Freeman, R.; Girsh, J.; Jou, A. F.-j.; Ho, J.-a. A.; Hug, T.; Dernedde, J.; Willner, I. *Anal. Chem.* **2012**, *84*, 6192−6198.
(118) Mandal, G.; Bardhan, M.; Ganguly, T. *J. Phys. Chem. C* **2011**, *115*, 20840−20848.
(119) Li, M.; Cushing, S. K.; Wang, Q.; Shi, X.; Hornak, L. A.; Hong, Z.; Wu, N. *J. Phys. Chem. Letters* **2011**, *2*, 2125−2129.
(120) Ray, P. C.; Fortner, A.; Darbha, G. K. *J. Phys. Chem. B* **2006**, *110*, 20745−20748.
(121) Gersten, J. I.; Nitzan, A. *Surf. Sci.* **1985**, *158*, 165−189.
(122) Griffin, J.; Singh, A. K.; Senapati, D.; Rhodes, P.; Mitchell, K.; Robinson, B.; Yu, E.; Ray, P. C. *Chem.–Eur. J.* **2009**, *15*, 342−351.
(123) Zhang, J.; Fu, Y.; Chowdhury, M. H.; Lakowicz, J. R. *J. Phys. Chem. C* **2007**, *111*, 11784−11792.
(124) Dyadyusha, L.; Yin, H.; Jaiswal, S.; Brown, T.; Baumberg, J. J.; Booy, F. P.; Melvin, T. *Chem. Commun.* **2005**, *25*, 3201−3203.
(125) Gill, R.; Willner, I.; Shweky, I.; Banin, U. *J. Phys. Chem. B* **2005**, *109*, 23715−23719.
(126) Liu, J.; Lee, J. H.; Lu, Y. *Anal. Chem.* **2007**, *79*, 4120−4125.
(127) Kim, Y. S.; Jurng, J. *Analyst* **2011**, *136*, 3720−3724.
(128) Li, M.; Wang, Q.; Shi, X.; Hornak, L. A.; Wu, N. *Anal. Chem.* **2011**, *83*, 7061−7065.
(129) Freeman, R.; Liu, X.; Willner, I. *Nano Lett.* **2011**, *11*, 4456−4461.
(130) Weizman, H.; Tor, Y. *J. Am. Chem. Soc.* **2001**, *123*, 3375−3376.
(131) Levine, L. A.; Williams, M. E. *Curr. Opin. Chem. Biol.* **2009**, *13*, 669−677.

(132) Schreiber, M.; Gonzalez, L. *J. Comput. Chem.* **2007**, *28*, 2299−2308.
(133) Daune, M.; Dekker, C. A.; Schachman, H. K. *Biopolymers* **1966**, *4*, 51−76.
(134) Pan, W.; Clawson, G. A. *Expert Opin. Biol. Ther.* **2008**, *8*, 1071−1085.
(135) Sigel, R. K. O.; Sigel, H. *Acc. Chem. Res.* **2010**, *43*, 974−984.
(136) Freeman, R.; Finder, T.; Willner, I. *Angew. Chem., Int. Ed.* **2009**, *48*, 7818−7821.
(137) Wu, C.-S.; Oo, M. K. K.; Fan, X. *Acs Nano* **2010**, *4*, 5897−5904.
(138) Zayats, M.; Willner, I. *Biosensing for the 21st Century*; Springer: New York, 2008; Vol. *109*, pp 255−283.
(139) Pardo-Yissar, V.; Katz, E.; Wasserman, J.; Willner, I. *J. Am. Chem. Soc.* **2003**, *125*, 622−623.
(140) Golub, E.; Pelossof, G.; Freeman, R.; Zhang, H.; Willner, I. *Anal. Chem.* **2009**, *81*, 9291−9298.
(141) Golub, E.; Niazov, A.; Freeman, R.; Zatsepin, M.; Willner, I. *J. Phys. Chem. C* **2012**, *116*, 13827−13834.
(142) Mao, C. D.; Sun, W. Q.; Shen, Z. Y.; Seeman, N. C. *Nature* **1999**, *397*, 144−146.
(143) Seeman, N. C. *Trends Biochem. Sci.* **2005**, *30*, 119−235.
(144) Nutiu, R.; Li, Y. F. *Angew. Chem., Int. Ed.* **2005**, *44*, 5464−5469.
(145) Beissenhirtz, M. K.; Willner, I. *Org. Biomol. Chem.* **2006**, *4*, 3392−3401.
(146) Bath, J.; Turberfield, A. J. *Nat. Nanotechnol.* **2007**, *2*, 275−284.
(147) Simmel, F. C.; Yurke, B. *Phys. Rev. E* **2001**, *63*, 041913.
(148) Liedl, T.; Sobey, T. L.; Simmel, F. C. *Nano Today* **2007**, *2*, 36−41.
(149) Teller, C.; Willner, I. *Curr. Opin. Biotechnol.* **2010**, *21*, 376−391.
(150) Yurke, B.; Turberfield, A. J.; Mills, A. P.; Simmel, F. C.; Neumann, J. L. *Nature* **2000**, *406*, 605−608.
(151) Chen, Y.; Wang, M. S.; Mao, C. D. *Angew. Chem., Int. Ed.* **2004**, *43*, 3554−3557.
(152) Shin, J. S.; Pierce, N. A. *J. Am. Chem. Soc.* **2004**, *126*, 10834−10835.
(153) Tian, Y.; He, Y.; Chen, Y.; Yin, P.; Mao, C. D. *Angew. Chem., Int. Ed.* **2005**, *44*, 4355−4358.
(154) Tian, Y.; Mao, C. D. *J. Am. Chem. Soc.* **2004**, *126*, 11410−11411.
(155) Wang, Z.-G.; Elbaz, J.; Willner, I. *Angew. Chem., Int. Ed.* **2012**, *51*, 4322−4326.
(156) Elbaz, J.; Shlyahovsky, B.; Willner, I. *Chem. Commun.* **2008**, 1569−1571.
(157) Elbaz, J.; Tel-Vered, R.; Freeman, R.; Yildiz, H. B.; Willner, I. *Angew. Chem., Int. Ed.* **2009**, *48*, 133−137.
(158) Liu, X.; Niazov-Elkan, A.; Wang, F.; Willner, I. *Nano Lett.* **2013**, *13*, 219−225.
(159) Lu, C.-H.; Wang, F.; Willner, I. *Chem. Sci.* **2012**, *3*, 2616−2622.
(160) Lu, C.-H.; Wang, F.; Willner, I. *J. Am. Chem. Soc.* **2012**, *134*, 10651−10658.
(161) Wang, F.; Elbaz, J.; Willner, I. *J. Am. Chem. Soc.* **2012**, *134*, 5504−5507.
(162) Shimron, S.; Wang, F.; Orbach, R.; Willner, I. *Anal. Chem.* **2012**, *84*, 1042−1048.
(163) Wang, F.; Elbaz, J.; Orbach, R.; Magen, N.; Willner, I. *J. Am. Chem. Soc.* **2011**, *133*, 17149−17151.